Kaunas University of Technology

Faculty of Mathematics and Natural Sciences

Investigation of Fluorescent Emitters Towards Efficient Hyperfluorescence Organic Light-Emitting Diodes

Master's Final Degree Project

Ervinas Urbonas

Project author

Chief Researcher dr. Dmytro Volyniuk

Supervisor

Kaunas, 2021

Kaunas University of Technology

Faculty of Mathematics and Natural Sciences

Investigation of Fluorescent Emitters Towards Efficient Hyperfluorescence Organic Light-Emitting Diodes

Master's Final Degree Project

Material Science (6211FX009)

Ervinas Urbonas

Project author

Chief Researcher dr. Dmytro Volyniuk

Supervisor

Prof. Dr. Tomas Tamulevičius

Reviewer

Kaunas, 2021

Kaunas University of Technology

Faculty of Mathematics and Natural Sciences

Ervinas Urbonas

Investigation of fluorescent emitters towards efficient hyperfluorescence organic light-emitting diodes

Declaration of Academic Integrity

I confirm the following:

1. I have prepared the final degree project independently and honestly without any violations of the copyrights or other rights of others, following the provisions of the Law on Copyrights and Related Rights of the Republic of Lithuania, the Regulations on the Management and Transfer of Intellectual Property of Kaunas University of Technology (hereinafter – University) and the ethical requirements stipulated by the Code of Academic Ethics of the University;

2. All the data and research results provided in the final degree project are correct and obtained legally; none of the parts of this project are plagiarised from any printed or electronic sources; all the quotations and references provided in the text of the final degree project are indicated in the list of references;

3. I have not paid anyone any monetary funds for the final degree project or the parts thereof unless required by the law;

4. I understand that in the case of any discovery of the fact of dishonesty or violation of any rights of others, the academic penalties will be imposed on me under the procedure applied at the University; I will be expelled from the University and my final degree project can be submitted to the Office of the Ombudsperson for Academic Ethics and Procedures in the examination of a possible violation of academic ethics.

Ervinas Urbonas

Confirmed electronically

Urbonas Ervinas. Investigation of fluorescent emitters towards efficient hyperfluorescence organic light-emitting diodes. Master's Final Degree Project / supervisor Chief Researcher dr. Dmytro Volyniuk; Faculty of Mathematics and Natural Sciences, Kaunas University of Technology.

Study field and area (study field group): Technology sciences (F), Technology of materials (F03).

Keywords: OLED, organic, semiconductors, hyperfluorescence, TADF.

Kaunas, 2021. 61 p.

Summary

In the recent years organic light-emitting diodes and organic semiconductors are getting a lot of attention in the industry. These devices have a number of distinct advantages, including a low cost, quick and easy manufacturing process, durability, optical clarity, and light weight. Despite OLEDs' recent commercialization, primarily in smartphone and television displays, their external quantum efficiencies still remain below the theoretical limit. It is primarily concerned with the properties of organic semiconductors (OLED emitters). Solid state photoluminescence quantum yield close to the 100 percent, good stability under electrical excitations, ability to harvest both singlet and triplet excitons, sufficient energy levels for hole and electron injections, and so on are all characteristics of a good emitter. However, achieving a perfect combination of the aforementioned properties is extremely difficult, particularly when dealing with heavy-atom-free compounds. The aim of this research was to look at new group of organic semiconductors and show their potential to be used in OLED applications as emitters. The main object of the study were four heavy-atom-free compounds based on mono and tetra phenothiazine substituted tetraphenylethylenes containing cyano groups. UV-Vis spectrometry, photoelectron emission spectrometry, and time of flight measurements were used in order to investigate the photophysical, electrooptical, and charge transporting properties of the studied compounds prior to OLED fabrication. All studied compounds were characterized by prompt fluorescence with aggregation-induced emission enhancement properties. The investigated compounds emit efficiently in the solid state, with intensity of photoluminescence maxima ranging from 464 to 575 nm and photoluminescence quantum yields ranging between 19-28 percent, while optical band gaps were calculated to be in the range of 2.32 – 2.88 eV. Aggregation-induced emission enhancement for studied phenothiazine substituted tetraphenylethylenes derivatives was proved by testing them in THF/water solutions. Photoelectron emission spectrometry revealed that ionization potentials of the studied compounds ranged from 5.48 to 5.63 eV, while time-on-flight measurements showed that all compounds only capable to transport holes with maximum holes mobility of 1.67×10^{-4} cm^2/Vs. Based on obtained results three different OLEDs' structures were fabricated using various fabrication techniques. The best OLED which had pure emission layer demonstrated maximum brightness of 4070 cd/m^2, maximum current efficiency of 5.70 cd/A and external quantum efficiency of 1.73 %. The best hyperfluorescence based device was characterized by maximum external quantum efficiency of 8.2 %, current efficiency of 21.58 cd/A and maximum brightness of 3400 cd/m^2.

.

Ervinas Urbonas. Fluorescencinių spinduolių tyrimai siekiant pagaminti efektyvius hiperfluorescencinius organinius šviesos diodus. Magistro baigiamasis projektas / vadovas dr. Dmytro Volyniuk; Kauno technologijos universitetas, Matematikos ir gamtos mokslų fakultetas.

Studijų kryptis ir sritis (studijų krypčių grupė): Technologijų mokslai (F), Medžiagų technologijos (F03).

Reikšminiai žodžiai: OLED, organiniai, puslaidininkiai, hiperfluorescencija, TADF.

Kaunas, 2021. 61 p.

Santrauka

Mūsų dienomis organiniai šviesos diodai ir organiniai puslaidininkiai sulaukia didelio pramonės susidomėjimo. Tokie prietaisai turi daugybė unikalių savybių, tokių kaip nebrangi, greita ir paprasta gamybos technologija, ilgaamžiškumas, optinis pralaidumas ir mažas svoris. Nepaisant to, kad organiniai šviestukai jau dabar plačiai naudojami gaminant telefonų ir televizorių ekranus, jų išorinis kvantinis našumas vis dar nesiekia maksimalios teorinės vertės. Pirmiausia tai lemia organinių puslaisininkių (OLED spinduolių) savybės. Artimas 100% fotoliuminiscencijos kvantinis našumas kietoje būsenoje galimybė išnaudoti tiek singletinius, tiek tripletinius eksitonus, stabilumas esant elektriniam žadinimui, tinkami energetiniai lygmenys skylių ir elektronų injekcijai yra tik keletas savybių, reikalingų geram organiniam spinduoliui. Tačiau pasiekti šių savybių kombinaciją yra labai sunku, ypač junginių, sudėtyje neturinčių sunkiųjų atomų, atveju. Šio tyrimo tikslas yra ištirti naują organinių puslaidininkių grupę ir parodyti jos patencialą būti pritaikytai kaip OLED spinduoliai. Šio tyrimo ašis buvo keturi mono ir tetra tetrafeniletilenu pakeisti pentiazino junginiai neturintys sunkiųjų metalų atomų. UV-Vis spektroskopija, fotoelektronų emisijos spektrometrija, lėkio trukmės matavimai - tai tik keletas iš metodų, kurie buvo panaudoti sienkiant nustatyti junginių fotofizikines, elektro-optines ir krūvio pernašos savybes. Visiems junginiams buvo būdinga sparti fluorescencija, kurią sustiprina agregatų susidarymas. Visi junginiai pasižymėjo efektyvia emisija kietoje būsenoje, su fotoliuminiscencijos maksimumais tarp 464-575nm ir 19-28% fotoliuminescencijos efektyvumais, kol draustinių juostų plotis buvo lygus 2,32-2,88 eV. Agregacijos sustiprintos emisijos reiškinys tirtiems junginiams buvo įrodytas ekperimento su vandens ir tetrahidrofurano tirpalais metu. Fotoelektronų emisijos spektrometrijos rezultatai parodė, kad junginių joninacijos potencialai yra lygūs 5,48-5,63 eV, kol lėkmio trukmės matavimai parodė, kad junginiams būdinga tik skylių transportacija, jų judriui siekiant iki $1,67 \times 10^{-4}$ cm^2/Vs. Naudojantis gautais rezultatais buvo pagamintos trys skirtingos organinių šviestukų struktūros, kurios skyrėsi ne tik struktūra, bet ir gamybos technika. Geriausias šviestukas su grynu tiriamos medžiagos emituojančiu sluoksniu pademonstravo 4070 cd/m^2 maksimalų skaistį, o maksimalūs srovės bei išorinis kvantinis našumas atitinkamai siekė 5,70 cd/A ir 1,73 %. Tuo metu geriausias prietaisas su hiperfluorescencine emisine struktūra buvo charakterizuotas 3400 cd/m^2 skaisčiu, kol maksimalus išorinis kvantinis našumas bei srovės efektyvumas atitinkamai siekė 8,2 % ir 21,58 cd/A .

Table of contents

List of figures

List of tables

List of abbreviations and terms

Abbreviations:

ACQ – aggregation-caused quenching
AIE – aggregation induced emission
AEE – aggregation enhanced emission
EBL – electrons blocking layer
EML – emitting layer
EQE – external quantum efficiency
ETL – electrons transport layer
HAT-CN – 1,4,5,8,9,11-Hexaazatriphenylenehexacarbonitrile
HBL – holes blocking layer
HOMO – highest occupied molecular orbital
HTL – hole transport layer
IC – internal conversion
ISC – intersystem crossing
ITO - indium-tin-oxide
LCAO - linear combination of atomic orbitals
LUMO – lowest unoccupied molecular orbital
mCP – 1,3-bis(9-carbazolyl)benzene
NPB – N,N′-Di(1-naphthyl)-N,N′-diphenyl-(1,1′-biphenyl)-4,4′-diamine
OLED – organic light emitting diode
PL – photoluminescence
PLQУ – photoluminescence quantum yield
RISC- reverse intersystem crossing
TADF – thermally activated delayed fluorescence
TAPC - 4,4′-cyclohexylidenebis[N,N-bis(4-methylphenyl)benzenamine]
THF – tetrahydrofuran
TOF – time-of-flight
TPBi – 2,2’,2’’-(1,3,5-benzinetriyl)-tris(1-phenyl-1-*H*-benzimi-dazole)
TSPO1 – diphenyl-4-triphenylsilyl-phenylphosphineoxide
TTA – triplet-triplet annihilation

Introduction

Since 1987 when Tang and Van Slyke invented first organic light-emitting diode (OLED) [1] organic semiconductors and OLEDs have attracted exceptional industrial interest particularly in the opto-electronics field. Nowadays organic small molecule semiconductors are used in various applications like data storage devices, security inks, solid state lasers, non-linear optics, lighting, solar cells, displays and much more [2]–[8]. These devices have a lot of exclusive advantages such as light weight, fast, simple and relatively cheap production technology and flexibility [9]. However, the fastest growing organic semiconductors field is OLEDs in particular their applications in lighting and displays. It is expected that OLEDs market will register compound annual growth rate of 12.9% over the five years period (2021 - 2026). With enhanced 8K (7680 x 4320 pixels) resolution, relatively new form factors, and larger screen sizes, OLEDs remain a significant display technology trend. For a long time, companies like Samsung and LG experimented with versatile OLED displays. Samsung, in particular, now makes all of its flagship devices with curved flexible OLED displays [10].

During organic semiconductors electroluminescence process electron–hole pair – exciton - is formed. This pair is a neutral quasi-particle bonded by the electrostatic Coulomb interaction. Since both, negatively charged electron and positively charged hole have spins, based in spin statistics four different spin combinations are possible: one combination of antiparallel spins, giving a singlet, and three combinations of parallel spins, giving a triplet [11]. Based on that singlet:triplet excitons ratio for organic semiconductor is 1:3 which creates statistical 25% limit for conventional fluorescent emitter internal quantum efficiency (IQE) while external quantum efficiency (EQE) is limited to around 5% despite that compound is characterized by photoluminescence quantum yield (PLQY) of 100% [12]. In order to access remaining 75% of excitons in triplet states, phosphorescent heavy metal atoms (e.g., Ir and Pt) containing complexes have been developed and used as emitters for the second generation of OLEDs. Strong spin-orbit interaction in these compounds creates very efficient intersystem crossing (ISC) which allows radiatively harvest triplet excitons resulting in 100% IQE of OLEDs. However, such organometallic systems suffer from a number of inseparable problems like toxicity, high price of metal-organic complexes instability, poor color purity and brightness [13].

Thus, the development of emitters that avoid the usage organometallic compounds is important. Triplet–triplet annihilation (TTA) is another way to produce additional singlet excitons. However, since this method can only convert 50 percent of triplet excitons into singlets, TTA can only achieve a maximum internal quantum efficiency of 62,5 percent [14]. One more popular alternative method is thermally activated delayed fluorescence (TADF) which is based on reverse intersystem crossing (RISC). During the RISC process, triplet excitons are converted to singlets, which then recombine in a radiative manner. Because of that TADF molecules are capable to reach 100% IQE and at the same time to avoid some disadvantages phosphorescent emitters have [15]. However, TADF emitters share many of the same problems as phosphorescent emitters, such as a short lifetime (especially for blue OLEDs) and a broad electroluminescence spectrum.

Hyperfluorescence is a relatively new technique for making effective use of triplet excitons in OLEDs, which also theoretically allows to reach 100 percent IQE. [16]. All hyperfluorescence systems are based on three elements: host, TADF molecules as co-hosts and fluorescent dopant. Hyperfluorescence solves multiple problems at once: in comparison to prompt fluorescence, hyperfluorescence allows to reach higher IQE and EQE of OLEDs while in comparison to TADF systems, this approach suggests higher operational stability and color purity of OLEDs [17].

Universal hyperfluorescence structure could be next big thing in OLEDs development. However, the topic is relatively new and universal hyperfluorescence systems have not been found yet which makes research on hyperfluorescence structures extremely important and relevant. The aim of this study is to determine photophysical characteristics of phenothiazine based tetraphenylethylene derivatives and to use them as emitters in hyperfluorescence-based OLEDs in order to obtain high external quantum efficiency. To achieve this aim following tasks will be completed:

1) Investigation of photophysical and electrooptical properties of tetraphenylethylene derivatives;
2) Development of working hyperfluorescence system using selected compounds;
3) Development of the hyperfluorescence OLEDs structure in order to get high device efficiencies (EQE > 5%).

1. Literature review

1.1. Molecular orbital theory

The state of a particle can be expressed by its wavefunction which can be found by using time independent Schrödinger equation:

$$\hat{\mathrm{H}}\psi^T = E\psi^T \tag{1.1}$$

where $\hat{\mathrm{H}}$ is the Hamiltonian, ψ^T is the total wavefunction and E is allowed energy eigenstates. Hamiltonian here has widely known expression:

$$\hat{\mathrm{H}} = -\frac{\hbar^2}{2m}\Delta - \frac{\hbar^2}{2M}\Delta - V\,(r, R) \tag{1.2}$$

Here Δ is the Laplacian in cartesian coordinates, while *m* and M is the mass of electron and nucleus, respectively. *V (r, R)* in this expression is the potential energy operator which depends on both - *r* and *R* (electron and nucleus positions) while the first two components are responsible for electron and nucleus kinetic contribution, respectively.

I order to make the computation of molecular wavefunctions and other properties for large molecules easier Born–Oppenheimer approximation is introduced. This approximation allows to treat wave functions of nucleus and electrons in a molecule separately, based on the fact that the nucleus is much heavier than the electron. In other words, with the same amount of kinetic energy, the nucleus moves much more slowly than the electron which allows to express total molecules wavefunction as the product of an electronic wavefunction and a vibrational wavefunction [18]:

$$\psi^T(r, R) = \psi^e(r) \cdot \psi^N(R) \tag{1.3}$$

However, in order to solve Schrödinger equation for systems with many electrons more approxiamtions are needed. Hartree-Fock approximation allows to reduce N-particle problem to a set of single particle equations that we know (in theory) how to solve [19]. Using this approximation total electron wave function can be expressed as follows:

$$\psi^e = \prod_i \psi_i \tag{1.4}$$

Where, ψ^e is total electron wavefunction and ψ_i single electron wavefunction.

Even with these approximations it is impossible to exactly calculate molecule orbitals for the most molecules, thus additional approximation called Linear Combination of Atomic Orbitals has to be introduced. According to this approach, the molecular orbitals can be written as a linear expression of atomic orbitals [20]. In the case of two hydrogen atoms, total wavefunction can be expressed as follows:

$$\psi_\pm = \psi_{1s}(A) \pm \psi_{1s}(B) \tag{1.5}$$

$$\psi_{1s}(A) = \sqrt{\frac{1}{\pi a_0^3}}\, e^{-r_a/a_0} \tag{1.6}$$

Here A and B are two separate hydrogen atoms, r_a is the distance between electron and hydrogen atom A. The wavefunction for hydrogen B is equal to (1.6) but with instead r_a, r_b is used. As a result of Linear Combination of Atomic Orbitals (1.5), two molecular orbitals have been obtained: $\psi_+ \; and \; \psi_-$ which stands for bonding and anti-bonding orbitals, respectively.

Bonding molecular orbital is a result of the sum of the atomic orbitals. This sum results in electron density higher than zero in between the two nuclei (see Fig 1.1) such configuration is energetically favorable because its energy is lower than of the isolated atomic orbitals. On the other hand, anti-bonding molecular orbital is the result of the difference between atomic orbitals. This difference resulting that electron density in the center between the nuclei is equal to zero (see Fig 1.1). Such configuration is energetically unfavorable for the molecule stability because its energy is higher than of isolated atomic orbitals.

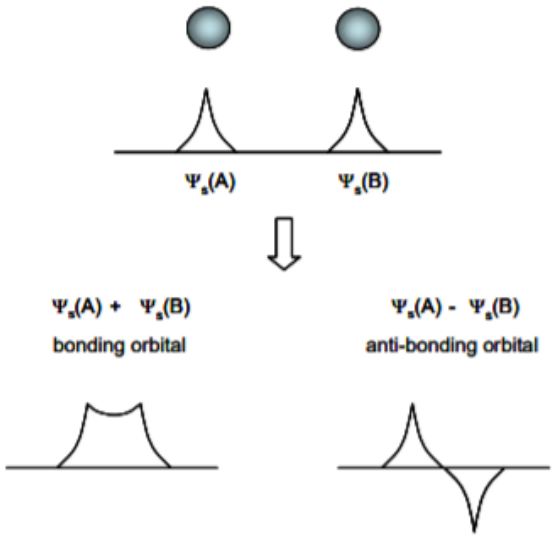

Fig. 1.1 Representation and wavefunction of the atomic orbitals (upper part in the figure) and the bonding and anti-bonding molecular orbitals (lower part) [19].

In Fig. 1.1 there are two electrons (each atom has one), in case of opposite spin (following Pauli exclusion principle [21]), both of the electrons will occupy the bonding orbital, which has the lower energy. Third and fourth electrons would occupy the anti-bonding orbital what would not be energetic favorable because total energy would be equal or higher than the sum of the of the separated atoms. For example, helium atoms have two valence electrons each and are more stable in their atomic form. In terms of a body consisting of many molecules, the sum of all of the molecular orbitals, results in a farther splitting (see Fig 1.2) with the appearance of bands structure. The highest occupied molecular orbital (HOMO) is the equivalent of valence band and the lowest unoccupied molecular orbital (LUMO) is the equivalent of conduction band in inorganic semiconductors. The difference between HOMO and LUMO corresponds to the band gap (E_g). For organic semiconductors this band gap is usually in between 1,5-3 eV [2]. It is responsible for the organic semiconductors photophysical properties such as emission and absorption. Organic semiconductors band gap can be modified by incorporation of various heteroatoms like oxygen or nitride and adding or reducing the number of aromatic rings [22].

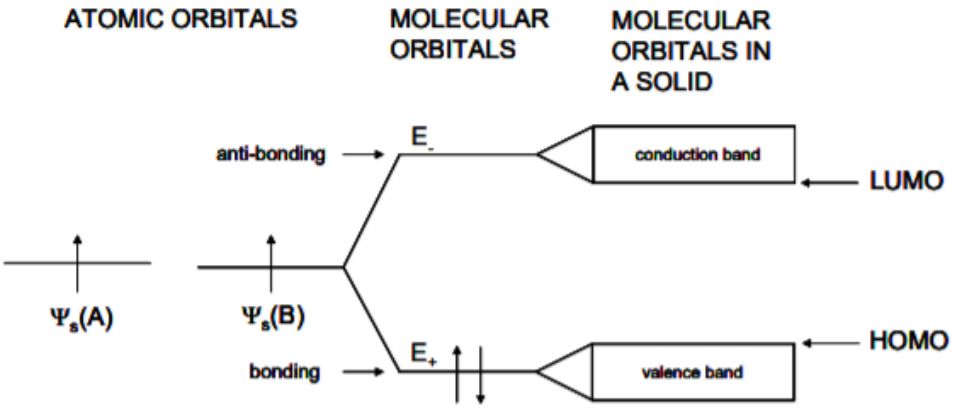

Fig. 1.2 Scheme of the energetic levels of separate atoms, molecule composed of two atoms and a solid from multiple molecules [19].

1.2. Excitons in organic semiconductors

In case of orgamic semiconductors, excitations can be created optically or electrically. In the first case after optical absorption electron is lifted from HOMO level into the LUMO level of the molecule, in the second case an electron and a hole are injected into material from electrodes. Such excitations forms a neutral quasi - particle - exciton, electron and hole pair coupled by Coulomb attraction [23]. In organic compounds, excitons are of the Frenkel type, localized on one or more molecules, and their energy is in the 0.1 - 1 eV range [2]. This is one of the main differences between organic and inorganic semiconductors, where the excitons are of the Wannier-Mott type with a small energy of several meV size [24]. Visual representation of Frankel and Wannier-Mott type excitons can be seen in Fig. 1.3 a [25].

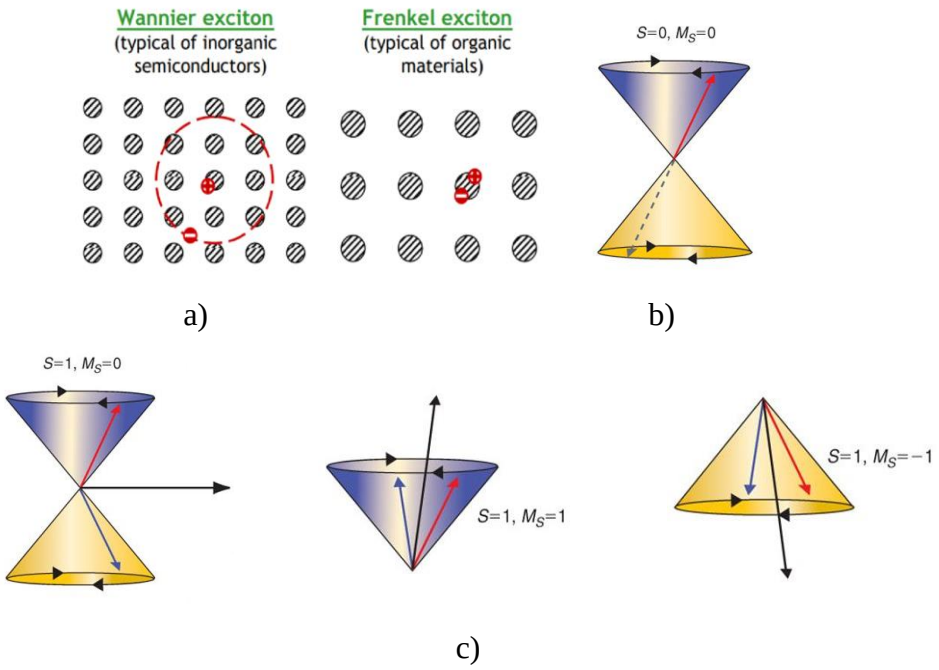

Fig. 1.3 a) Visual representation of Frankel and Wannier-Mott type excitons, b) vector representation of singlet, c) vector representation of triplet [24]

Moreover, excitons in organic semiconductors can be divided into two additional classes: singlet and triplet excitons depending on the spin of particles. Each electron has a spin which is a vector, but is often expressed as a projection on the z axis.. For a particle like electron, spin projection on z axis can be equal to 1/2 or -1/2 , which also often called as "spin up" or ↑ and "spin down" or ↓, respectively. According to Pauli exclusion principle electrons occupy filled molecular orbitals in pairs: one electron with spin 'up' and one electron with spin 'down' [21].

Wavefunction which describes an electron can be divided into two parts: spatial part $\psi_a(r_1)$ and spin part $\psi_{spin}(s_1)$:

$$\psi_a(r_1, s_1) = \psi_a(r_1) \cdot \psi_{spin}(s_1) \quad 1.7$$

$$\psi_{spin}(s_1) = \begin{pmatrix} 1 \\ 0 \end{pmatrix} = \uparrow \; or \; \psi_{spin}(s_1) = \begin{pmatrix} 0 \\ 1 \end{pmatrix} = \downarrow \quad 1.8$$

If the molecule has closed shell that means that all electrons in ground state is paired and in case of excitation, excited electron can be coupled with the electron which left unpaired in the ground state. The wavefunction of such excited state can be considered as a wavefunction of the two unpaired electrons and expressed in the same way like in case of one electron:

$$\psi_a(r_A, r_B, s_A, s_B) = \psi_a(r_A, r_B) \cdot \psi_{spin}(s_A, s_B) \quad 1.9$$

According to Hilbert space formalism these electrons are indistinguishable and interchanging of these two electrons will not change the probability density:

$$|\psi(A, B)|^2 = |\psi(B, A)|^2 \quad 1.10$$

Therefore the overall wavefunction of these electrons must be antisymmetric in the case of their exchange: $\Psi(A,B) = -\Psi(B,A)$. Because of that one of parts of this wavefunction (spatial or spin part) has to be antisymmetric while the other one is symmetric.

$$\psi(r_A, r_B, s_A, s_B) = \begin{cases} \psi^A(r_A, r_B) \cdot \psi^S{}_{spin}(s_A, s_B) \\ \psi^S(r_A, r_B) \cdot \psi^A{}_{spin}(s_A, s_B) \end{cases} \quad 1.11$$

where S and A stands for symmetric and antisymmetric wavefunctions. It two electron wavefunction can be expressed in four different variations (see Fig 1.3 b, c and Fig. 1.4):

1. Symmetric spatial part of the wavefunction and antisymmetric spin part which stands for singlet excited state. In case of singlet excited state total spin S equal to 0 which leads that $m_S = 0$ too;
2. Antisymmetric spatial part of the wavefunction and symmetric spin part (A="spin up" and B="spin up") which results in total spin S equal to 1 and $m_S = 1$;
3. Antisymmetric spatial part of the wavefunction and symmetric spin part (A="spin down" and B="spin down") which results in total spin S equal to 1 and $m_S = -1$;
4. Antisymmetric spatial part of the wavefunction and symmetric spin part (A="spin up" and B="spin down", but spatial part is antisymmetric so spins are "out of phase") which results in total spin S equal to 1 and $m_S = 0$;

Options 2-4 are called triplets. The total spin quantum number S for a triplet in all cases is equal to 1, which means that three states with m_S equal to +1, 0 or -1 are possible (see Fig. 1.4)

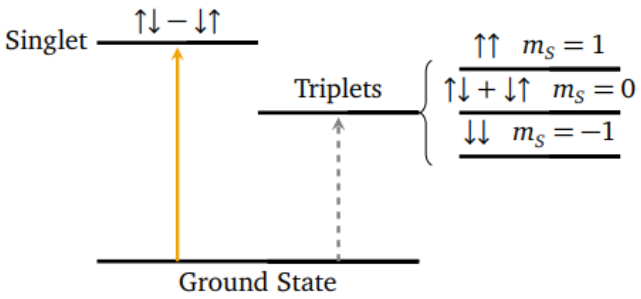

Fig. 1.4 Visualization of possible spins alignments during organic molecule excitation (singlet and triplet states) [26]

During OLED operation electrons are injected into organic layers resulting in equal probabilities of electron ending in one of four mentioned configurations. Based on that singlet:triplet excitons ratio for organic semiconductor is 1:3 which limits radiative decay of the compound because of different lifetime of these states [26].

1.3. Energy transfer in organic semiconductors

Excitons can move through organic semiconductors. Energy can be transferred radially when the donor molecule irradiates photon, the acceptor molecule can absorb this photon if the luminescence and absorption of these molecules' spectra overlap. Resonant transfer mechanisms such as Foster and Dexster also often take place in energy transfer of organic semiconductors.

Foster transport usually operates over short distances (~ 1 nm) and is limited to being able to transport only singlet excitons. It is radiationless exciton transfer process which does not involve light emission from donor to the acceptor molecule at any point instead it employs Coulombic dipoles interaction. During this process electron of the donor in the excited state moves setting up an oscillating dipole which induces an alternating electric field. This oscillating electric field then creates a dipole on one of the acceptor molecules causing coupling between donor and acceptor molecules. In order to this coupling be efficient and result in promotion of electron to an excited state on acceptor, oscillating electric field must be in resonance with an electron in that acceptor molecule. In addition, for transfer to be efficient emission spectra of donor molecule has to overlap with absorption spectra of acceptor [27]. After the transfer is over (acceptor electron is promoted) the electron in the excited state donor relaxes back to the ground state in that way minimizing the probability of back transfer. The whole process can be summarized as equation 1.12 or figure 1.5 b.

$$D^* + A \rightarrow D + A^* \qquad 1.12$$

Where * stands for excited state, D – molecule of donor and A – molecule of acceptor.

Foster energy transfer can work as effective radiative decay pathway for the donor molecule thus influencing lifetime of excited state. One example of that could be if donor molecule has two competing decay pathways – one radiative and one non-radiative – then it is possible quickly transfer energy to acceptor molecule which is effective emitter in that way bypassing non-radiative decay pathway. Moreover, such energy transfer enables efficient color tuning possibilities as shown in figure 1.5 b.

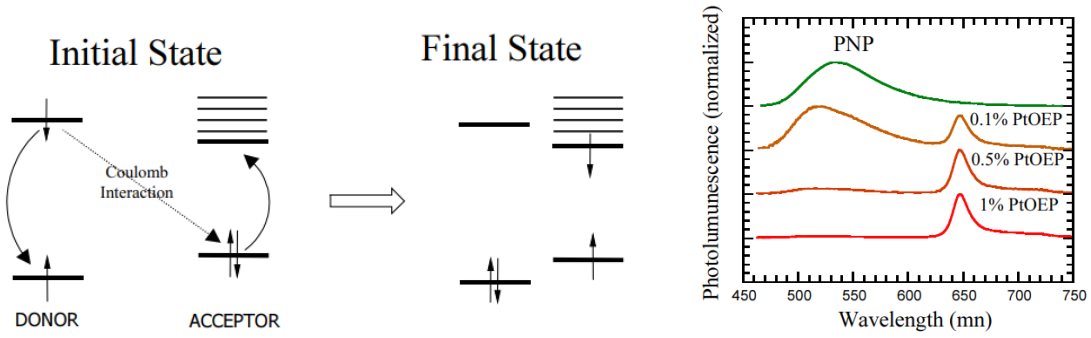

a) b)

Fig. 1.5 a) Visualization of Foster energy transfer, b) visualization of color-tuning by adding acceptor molecules into donor matrix.

Meanwhile, Dexster's energy transfer can take place over longer distances (~ 10 nm) in comparison to Foster energy transfer. Another difference from Foster transfer is that Dexter energy transfer is capable to operate both – singlet and triplet excitons. Mechanism of Dexter energy transfer is based on electron exchange (tunneling) process when excited state electron in donor molecule is swapped with ground state electron of acceptor molecule. These exchanges can either occur one after another (there ions are generated in the middle of the process) or in concerted way (Fig 1.6). As it is clear from mechanism itself Dexter energy transfer limitation is that spatial overlap of the electronic wavefunction in donor and acceptor is required. In addition, this mechanism also limited and by distance between donor and acceptor [28].

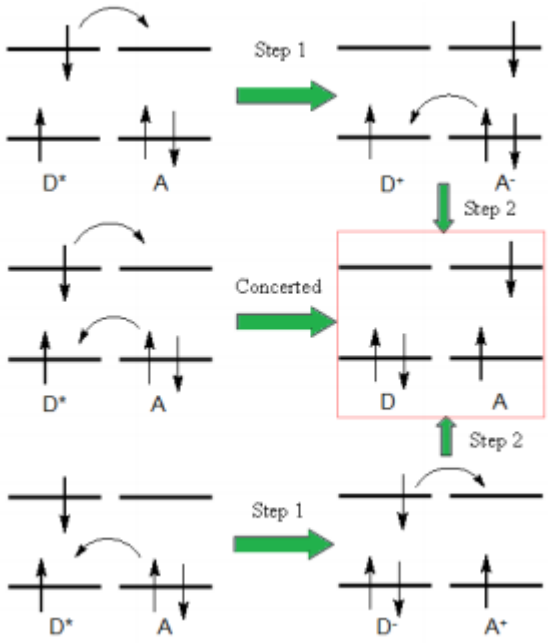

Fig. 1.6 Visualization of Dexter energy transfer pathways [28]

The rate of the Dexter energy transfer is exponential function of the distance between donor and acceptor. Because of that transfer rate is very sensitive to the change of distance between molecules then way are being moved apart. This bigger influence of the distance between acceptor and donor molecules on the rate of Dexter energy transfer as compared with Foster transfer is self-explanatory then mechanisms of the processes are taken into account. As mentioned, rate of Dexter energy transfer

exponentially depends on the distance between molecule while rate of Foster energy transfer depends as $1/R^6$ on the same factor. Relative visualization of Dexter and Foster energy transfers rate dependency on intermolecular distance is shown in figure 1.7.

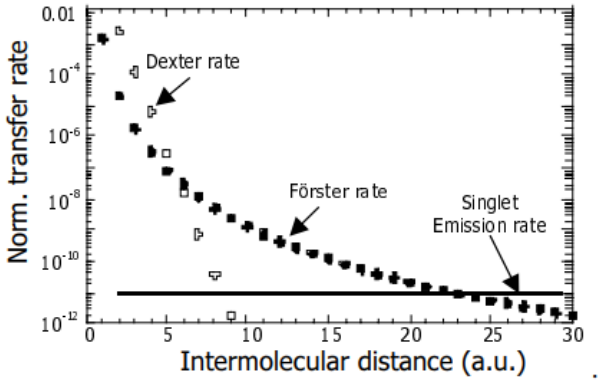

Fig. 1.7 Relative distance dependence of Foster and Dexter transfer [28]

Radiative energy transfer mechanism can be divided into two steps. During first step excited donor molecule decays radiatively resulting creation of photon. During the second step acceptor molecule absorbs that light which was emitted in the first step. Whole mechanism can be described by following equations:

$$D^* \rightarrow D + h\nu \qquad 1.13$$

$$A + h\nu \rightarrow A^* \qquad 1.14$$

Where hν in an energy of photon. From described mechanism it becomes obvious that for this energy transfer mechanism it is very important that luminescence and absorption spectra of donor and acceptor molecules would overlap.

1.4. Prompt fluorescence and phosphorescence

Luminescence is an emission of light by certain materials which is not related to blackbody radiation. By excitation form luminescence can be divided to chemiluminescence (excited by chemical reaction), bioluminescence (excited by chemical reactions in live organisms), triboluminescence (excited by mechanical changes in material), electroluminescence (excited by applied electric field), photoluminescence (excited by light), etc [29]. Photoluminescence is a process when a material is being exposed to incident radiation and as a result some of its energy is absorbed and re-emitted as a light of a longer wavelength. The light which is emitted can be visible light, infrared or ultra-violet light. Such difference between incident and re-emitted light wavelength is explained by Stokes law [30]. Mechanism of photoluminescence is usually divided into two steps: first – material excitation by light when electronic system is being excited to higher energy state, second – relaxation when electronic system returns to the ground state resulting emission of the photon or simply light. Characteristic photoluminescence time - τ_c – is a time between absorption of radiation and emission and is usually used as parameter allowing to classify photoluminescence phenomena into fluorescence and phosphorescence. If this time is lower than 10^{-8}s ($\tau_c<10^{-8}$s) the process is called fluorescence and if characteristic time is higher than 10^{-8}s ($\tau_c>10^{-8}$s) process then is called phosphorescence. Phosphorescence itself also can be divided into two main groups: short period ($\tau_c<10^{-4}$s) and long period phosphorescence ($\tau_c>10^{-4}$s). Thermoluminescence is a separate category of long period phosphorescence with extremely long characteristic photoluminescence time from

several minutes until years. Visualization of luminescence sub-groups by characteristic time can be seen in figure 1.8 [31].

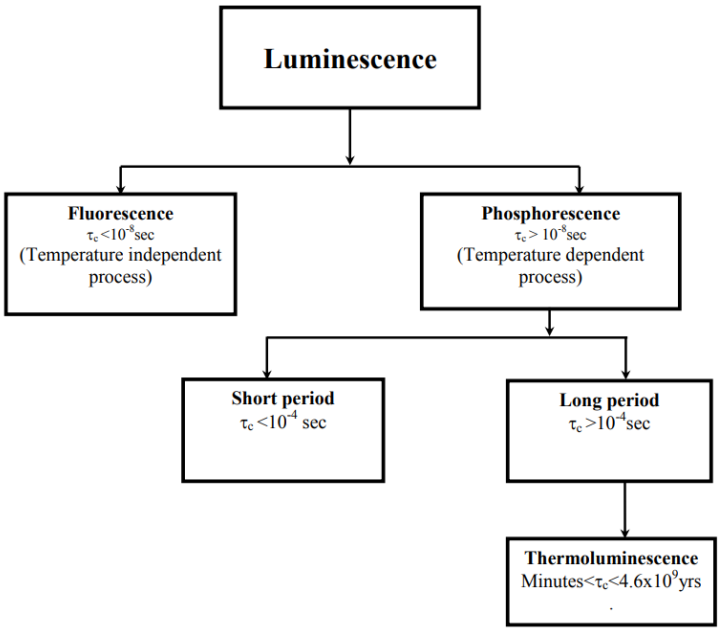

Fig. 1.8 Luminescence classification on duration time

Fluorescence is radiative spontaneous process when emission of light is seen to be taking place together with absorption of radiation and stopping immediately as radiation is over. One important thing about fluorescence is that multiplicity of spins in initial state is the same as in final state. [32]. Full process mechanism from light absorption until radiative relaxation can be visualized by Jablonski diagram (Fig 1.9 a). First transition in all photoluminescence processes is the absorbance of light of a specific energy (wavelength) by particular molecule. This transition is indicated by a straight violet arrow pointing up. Absorption is a very rapid transition, on the order of 10^{-15} seconds. During light absorption an electron is excited from a ground state (S_0) into one of the excited electronic states (S_1, S_2, S_3...) excited vibrational state (V_1, V_2, V_3...). After electron is excited, there is a number of possible relaxation methods. One of them is non-radiative process called intramolecular vibrational relaxation or IVR. It is also very fast process, between 10^{-14} and 10^{-11} seconds and because of that , it is extremely likely to happen immediately after absorption [33]. After electron changes its vibrational mode, relaxed energy is converted into kinetic energy (heat) which can stay within the same molecule or can be transferred to the molecules which are around. During IVR relaxation usually occurs only between vibrational levels, thus electron will not change its electronic energy state from one to another through this process. Another kind of non-radiative relaxation mechanisms is called internal conversion (IC). When vibrational energy levels strongly overlap electronic energy levels, IC occurs, allowing electrons to relax from one electronic state's vibrational level to another (lower) electronic state's vibrational level. It's seen as a curved green line between two vibrational levels in separate electronic states on the Jablonski diagram. IC occurs in conjunction with IVR and is a common way for molecules to release energy produced by light excitation. However, because of the large energy difference between the ground state (S_0) and the first electronically excited state (S_1), IC here is very slow, allowing other relaxation pathways to compete at the first electronically excited state. One of those pathways is fluorescence. It is indicated (Fig. 1.9 a) as a straight red line going down from first excited state to the ground state. It is relatively slow process between 10^{-9} and 10^{-7} seconds. This radiative transition from S_1 to S_0 is classified as a spin-allowed transition. However, it is not a very

likely electron energy relaxation pathway and occurs only at the first excited state because at higher excited states it is usually losing to IC and IVR due to the lower speed. Fluorescence emission is usually measured over range of wavelengths because of number of vibrational levels couples in the transition.

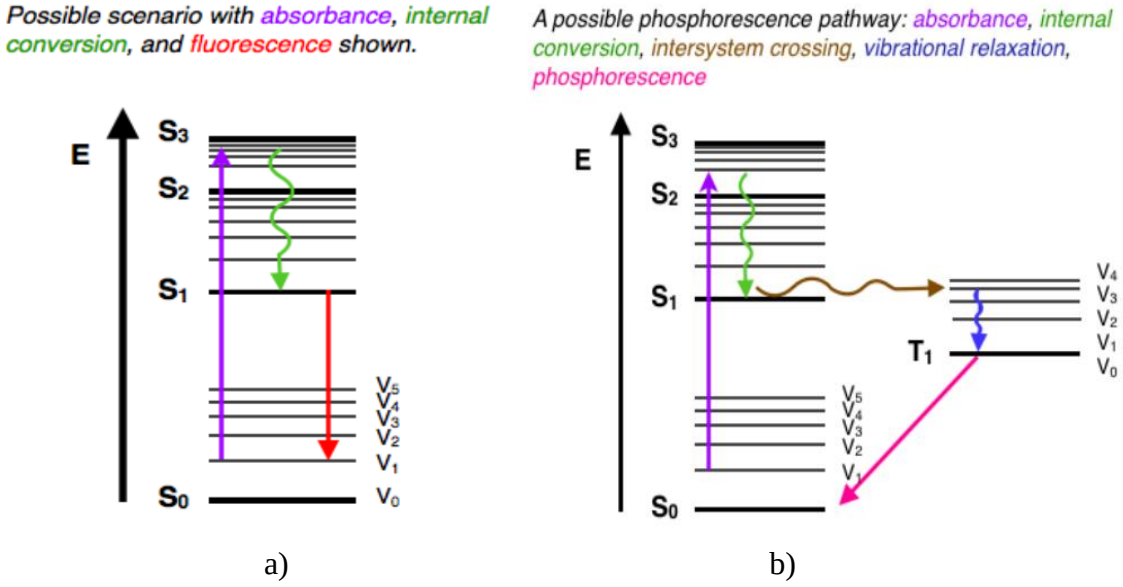

a) b)

Fig. 1.9 a) Schematic of fluorescence, b) schematic of phosphorescence [35]

Differently than fluorescence, phosphorescence is characterized by delay between absorption and time until emission reach its full intensity. Moreover, emission from phosphorescence can be visible for some time even excitation source has been removed. During phosphorescence excited electron relaxes from first exited triplet state to the ground state which means that process is spin-forbidden [34]. Because of that it is relatively slow process which means that other relaxation mechanisms usually dominate over it. However, it still can be observed at low temperatures or in case heavy-metal atoms are introduced into the molecule [35]. Schematic of all radiative and non-radiative transitions during phosphorescence emission can be seen in Jablonski diagram (Fig. 1.9 b). The beginning of the process is identical to the fluorescence: molecule is excited by external light source, after that non-radiative relaxation events – IVR and IC – take place. However, in case of fluorescence additional non-radiative transition called intersystem crossing (ISC) has to be introduced. It is an non-radiative transition when electron changes spin multiplicity from an excited singlet (S_1) state to an excited triplet state (T_1) which is also a slow, spin-forbidden transition [36]. In Jablonski diagram it is indicated by a horizontal, brown, curved arrow from one column to another. ISC is usually followed either by radiative transition (phosphorescence) or non-radiative deactivation. Non-radiative deactivation includes such processes as energy transfer between molecules through molecular collisions or quenching. However, under specific circumstances (low temperature or heavy-metal atoms) radiative phosphorescence can dominate over these transitions. In Jablonski diagram phosphorescence is indicated by a horizontal pink straight arrow from one column to another which again means that transition is spin-forbidden.

Jablonski diagrams shows a variety of possible radiative and non-radiative transitions during excitation and relaxation of the molecule. However, the probability of each transition to happen depending on time scale of that transition – the higher transition speed, the higher probability for it to happen. Because of that it is very beneficial to understand time scales of each transition in order to

estimate its possibility. Bellow is provided a table with time scales of most common transitions which were described before.

Table 1. Time scales of most common transitions

Transition	Time scale	Is transition radiative?
Absorbtion	10^{-15} s	Yes
Internal Conversion	10^{-14} - 10^{-11} s	No
Vibrational Relaxation	10^{-14} - 10^{-11} s	No
Fluorescence	10^{-9} - 10^{-7} s	Yes
Intersystem Crossing	10^{-8} - 10^{-3} s	No
Phosphorescence	10^{-4} - 10^{-1} s	Yes

1.5. Thermally activated delayed fluorescence

Mechanism of thermally activated delayed fluorescence (TADF) has improved considerably since 1961 when this photophysical process was first reported [37]. Using this mechanism, the first TADF-based OLED without heavy-metals was reported in 2012 [38] . Since then, the TADF mechanism has attracted considerable interest, for harvesting triplet states in metal-free organic materials for application in OLEDs [39]. In terms of lifetime TADF is right in the middle between prompt fluorescence and phosphorescence – usually in the range of several microseconds. The main transitions of TADF mechanisms is visualized by Jablonski diagram, there solid lines stand for radiative decays and dash lines stand for non-radiative decays (Fig. 1.10).

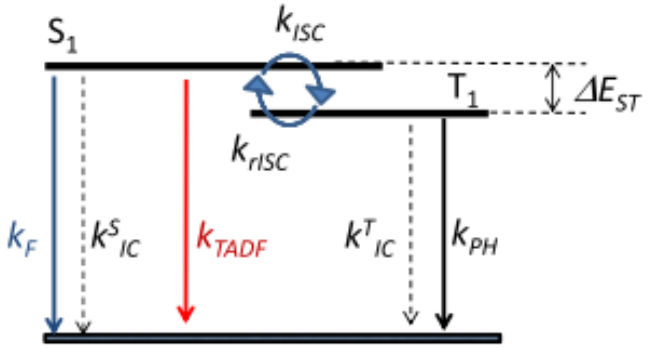

Fig. 1.10 Visualization of TADF machanism [40]

Like in all processes which were described before, firstly, the molecules are excited via absorption of external light. After absorption there are three different possibilities: a) radiative emission yielding prompt fluorescence, b) non-radiative decay or c) ISC to the triplet states. During TADF mechanism third option has to be the case. In other words, the start of TADF is identical to the phosphorescence. As excitons enter the triplet states, they can either recombine to the ground state through radiative or non-radiative emissions, or they can flip back to the singlet state. Reverse intersystem crossing (RISC), which is the cornerstone of the TADF mechanism, is the phenomenon by which the triplet state flips back to the singlet state. In order to lift the triplet state to a vibronic sub-level that is isoenergetic with the emissive singlet states in the case of TADF, only thermal energy is needed. This singlet →triplet →singlet cycle can be repeated several times until radiative decay from excited singlet state finally takes place [40]. The energy splitting between singlet and triplet states (ΔE_{ST})

should be as minimal as possible for TADF to work (less than a few hundreds of meV but ideally less than a few tens of meV for efficient RISC).Only in that case the rate of RISC will be higher that of phosphorescence or non-radiative decays from triplet states which is needed in order to up-convert most of the triplet states back to the singlets. The rate constant of RISC can be described as follows:

$$k_{RISC} \approx \frac{1}{3} exp\left(-\frac{\Delta E_{ST}}{kT}\right) \tag{1.15}$$

where k stands for s the Boltzmann constant and *T* is temperature. From this equation becomes clear that small ΔE_{ST} enhances the rate of RISC and triplet-to-singlet transition efficiency, which enhances the internal quantum efficiency (IQE) of TADF emitters. From the theoretical point of view, if ΔE_{ST} is small enough, the IQE of the TADF operation can reach even 100%. However, TADF based devices still has some disadvantages as wide emission spectra or poor operation stability.

1.6. Hyperfluorescence

Hyperfluorescence is a new technique for harvesting triplet excitons in OLEDs that theoretically allows 100% internal quantum efficiency. Here TADF molecules are used as an assistant dopant in fluorescent dopants and large bandgap host systems which in a center of hyperfluorescence structures [41]. The hyperfluorescence method allows to solve several problems at once. When compared to traditional fluorescence systems, hyperfluorescence implies higher internal quantum efficiencies and, as a result, higher external quantum efficiencies of OLEDs. When compared to TADF systems, hyperfluorescence allows to achieve higher color purity and, more importantly, better operational stability. (see Fig. 1.11) [16], [17], [41].

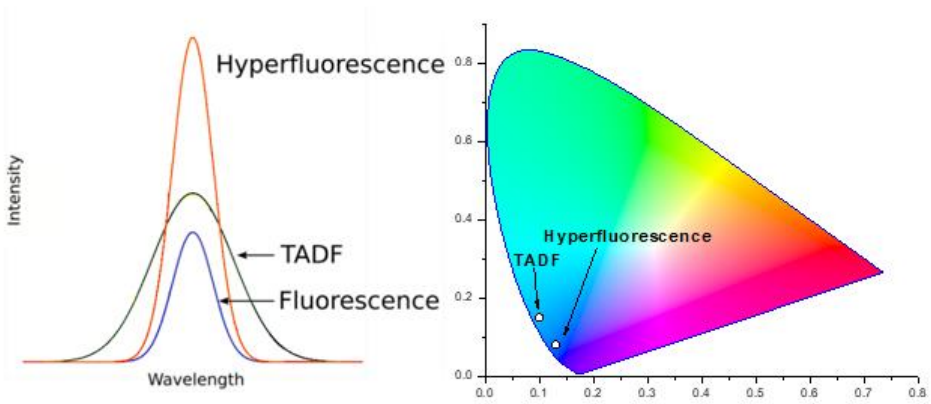

Fig. 1.11 Representation of hyperfluorescence systems properties [41]

Mechanism of hyperfluorescence consist of several main steps (see Fig. 1.12). Firstly, like in all mechanisms described above, molecule is excited by external energy source. The charge carriers are then transported on the large band gap host molecules before being trapped on the assistant dopant (TADF molecule) due to its shallower HOMO and deeper LUMO than of the host material. Once charges reach assistant dopant, triplet excitons created on TADF molecules are converted into singlet via effective RISC. The singlet excitons of the TADF molecule are transferred to the singlet state of the fluorescence dopant via Förster resonance energy transfer after being transformed from triplet to singlet via RISC. The photons are then emitted with high efficiency and narrow bandwidth from the fluorescent emitter. Each of these processes has a chance of decaying to the ground state without generation of light [16].

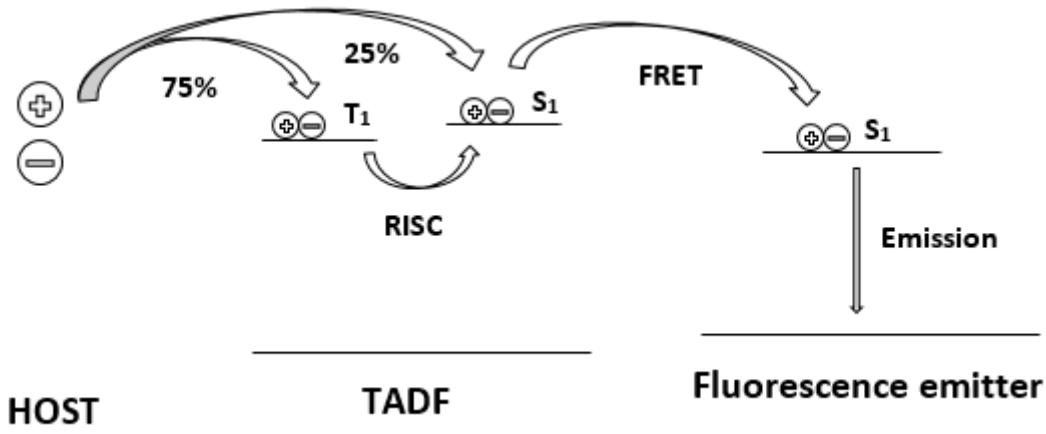

Fig. 1.12 Schematic of hyperfluorescence

In order to construct an efficient hyperfluorescence structure several requirements have to be fulfilled [16], [41], [42]:

1. The HOMO and LUMO of the host molecule must be lower than those of the TADF molecule, while the TADF molecule must have a larger energy difference than the fluorescent emitter. As a result, host materials with a high HOMO level are essential;
2. The ground state absorption of the fluorescent molecule and the emission of the TADF molecule should have a large spectral overlap in order to ensure effective FRET.;
3. To prevent direct trapping of charge carriers on fluorescent molecules, low fluorescent emitter doping concentrations (0.1-2%) and much higher TADF emitter concentrations (10-60%) must to be used.
4. To ensure that the TADF materials have a short decay time, the assistant dopant should have a high RISC rate;
5. If structures are formed by solution processing materials solubility and films surface roughness should be taken into account.

While hyperfluorescence is most commonly used in order to boost the EQE of single color fluorescent OLEDs, it also can be used in order to fabricate white OLED devices [43]. Although most hyperfluorescence WOLEDs are produced with a single emission layer and two fluorescent emitters [44], [45], in this work I will propose a novel method for fabricating hyperfluorescent WOLEDs with two separate emission layers.

1.7. Structure and working principle of organic light emitting diodes

OLEDs, unlike conventional light emitting diodes, are formed using organic compounds. These organic compounds are molecular carbon derivatives that are widespread on Earth and capable of forming a number of different molecular structures, bonding to both metal or phosphorus, and other derivatives and may therefore have different physical properties. Organic substances found both naturally in nature and synthesized in the laboratory. This leads to their wide range of use in the production of various different layers of organic light emitting diodes [46]. In the formation of an OLED, several organic layers are usually formed between the anode and the cathode (2 to 7 layers). The whole device is usually formed on transparent substrate. This multi - layer LED structure ensures that recombination of injected holes and electrons will appear in the main, emissive layer [47]. The structure of conventional OLED you can see in Fig. 1.13 a [48].

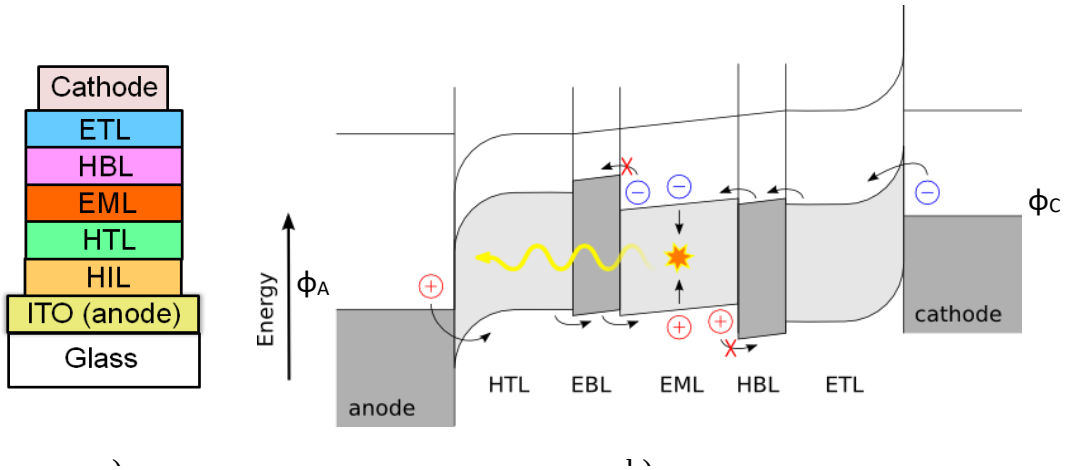

Fig. 1.13 a) conventional OLED stucture, b) basic working pronciple of OLED [47]

When manufacturing an OLED structure, it is important to select the right materials and prepare them properly:

1. Substrate: The most commonly used material for the substrate is glass. It is so popular because glass has excellent optical and mechanical properties: it is transparent, strong, has smooth surface and high resistance to chemical other and external effects. Not only selection of material but substrate preparation also has a significant impact on the performance of OLEDs - cleanliness is extremely important in substrates preparation.
2. Anode: Generally, the anode, like the substrate, must be transparent, so for this purpose indium tin oxide (ITO) is usually used [49]. It has a high conductivity, temperature resistance, transparency and high work function [50].
3. Hole and electron injection layers: To improve the injection of charge carriers, organic hole injection layer (HIL) or electron injection layers (EIL) with correspondingly low HOMO or high LUMO energy levels can be used. For this purpose such materials as platinum or copper phthalocyanine are usually used.
4. Hole transfer layer: In order for the injection of holes in this material to be effective, it must have good hole conductivity and high ionization potential I_c, it must be thermally stable, and also the hole work function Φ_m must be coordinated with the anode work function. To form hole transfer layer (HTL) or HIL such materials as α-NPD (N, N'-bis (naphthalen-1-yl) -N, N'-bis (phenyl) -2,2'- dimethylbenzidine), mCP (1,3-bis (carbazol-9-yl) benzene), TPD (N, N'-bis (3-methylphenyl) -N, N'-bis (phenyl) -benzidine), m-MTDATA (4,4 ', 4 ′ ′ - tris [phenyl (m tolyl) amino] triphenylamine), TAPC (di- [4- (N, N-di-p-tolylamino) - phenyl] cyclohexane), NPB (N, N'-bis (naphthalen-1-yl) -N, N'-bis (phenyl) -benzidine) are usually used. These materials have good hole drift mobility (~ 10-3 cm^2 / (Vs) [51]) and high ionization potential.
5. Electron transfer layer (ETL): EIL and ETL materials should be characterized by low electron-affinities which enables efficient electron injection, and high electron drift mobility. Because organic compounds are usually holes dominant, ETL materials are rarer. As EIL and ETL most commonly are used different metals chelates, oxadiazole compounds, pyridine [52], triazine compounds [53] and similar. One of the most popular materials is Alq3 (three (8-hydroxy-quinoline) aluminum). Also commonly used is BCP (2,9-dimethyl-4,7-diphenyl-1,10-phenanthroline), Bphen (4,7-diphenyl-1,10-phenanthroline), PPT (2,8- bis (diphenylphosphoryl) dibenzo [b, d] thiophene), TPBi (2,2 ', 2 "- (1,3,5-benzynethyl) - tris (1-phenyl-1-H-

benzimidazole) and TmPyPB (1,3,5-tri [(3-pyridyl) -phen-3- il] benzene). Electron mobility, compared to hole mobility, is usually smaller by at least a row as in the case of Bphen (μ_h = ~ 10^{-3} cm^2 / (Vs) while μ_e = ~ 10^{-4} cm^2 / (Vs) [54]), but also it can be much lower like in case of Alq3 (μ_e = 10^{-6} - 10^{-5} cm^2 / (Vs) [55]) and BCP (μ_e = 7-9 × 10^{-6} cm^2 / (Vs) [56]).

6. Emission layer (EML): EML usually consist of a mixture of two organic substances, where emissive material ("guest") is evaporated together with a wider energy gap compound (‘host’). Concentration of emissive substance usually is around 3-10% to avoid unwanted fluorescence concentrative quenching, as well as to effectively localize excitation. The "guest" and "host" systems are selected according to the color the OLED is being made: the "host" is always chosen with higher triplet energy for efficient localization of excitons in emissive material. The most popular emissive materials are various anthracene, carbazole, fluorene and pyrene compounds, while as ‘host’ substances are the most commonly used compounds, as mCP, DPEPO, PPT, TCTA (4,4 ', 4 "-tris (carbazol-9-yl) triphenylamine), CBP (4,4'-bis (carbazol-9-yl) biphenyl), CzSi (9- (4-tert-butylphenyl) -3,6- bis (triphenylsilyl) -9H-carbazole) with UGH-2 (1,4-bis (triphenylsilyl) benzene). All of them are characterized by high triplet energies, e.g. mCP, E_T = 2.9 eV, DPEPO, E_T = 3.1 eV [57]). The materials of the UGH family are characterized by particularly high triplet levels ($E_T \approx 3.5$ eV [58]) and can therefore be efficient used even with blue emitters.
7. Electron and holes blocking layers (EBL and HBL): Because the carriers are of different charges, they also migrate and spread in the surrounding layers. So to avoid for recombination and radiation in the non-emissive layer, the minimum layer thickness is important. A thin layer that blocks electrons and holes helps regulate charge transfer.In order to be efficient, EBL and HBL should be characterized by quite high LUMO and hole mobility and quite high electron mobility and HOMO, respectively.
8. Cathode: Commonly used metals with low electron work function, high conductivity and resistance to temperature and external influences.

A simplified two-layer structure consisting of conductive and emitting layers can be used to describe the working principle of OLEDs. When the voltage is connected to OLED (positive at the anode and negative at the cathode), holes and electrons will be injected from different electrodes and in some order charge carriers will be a transferred to the emission layer. Electrons and holes drift towards each other thus entering the heterojunction region where they are localized and bound to excitons. Exciton formation and radiative or non-radiative recombination occur in the emission layer, where the charge carriers are imprisoned in a potential well. Part excitons which recombines in the EML emit light [2]. The wavelength of the radiation depends on material HOMO and LUMO energy differences. According to Fig. 1.13b several processes necessary for the operation of the OLED can be distinguished:

1. Charge carrier injection: electrons are injected from the cathode material (usually Al) while for injection of holes ITO the material is usually used. The injection of holes and electrons takes place through a triangle of energy barrier.
2. Charge carrier transfer: this process is influenced by external and internal electric fields. The heterojunction formed at the point of contact of the organic layers improves the injection of the carriers and thus itself regulates transfer in the emissive layer [59].
3. Binding of charge carriers to excitons: the generation of excitons is determined by the density of localized carriers in the emission layer.

4. Recombination of excitons: Charge carriers bounded to the exciton state recombine by radiating energy (electroluminescence). The rate of recombination directly depends on mobilities of electron and hole motions:

$$r \sim \frac{e}{\varepsilon\varepsilon_0}(\mu_e + \mu_h) \quad 1.15$$

Where e is a charge of carrier and μ_e and $\mu_h$is mobility of electrons and holes, respectively.

1.8. Organic light emitting diode efficiency

The parameters of an OLED are determined by both the structure of the device itself and the properties of functional layers‘ molecules. OLED derivative external quantum efficiency (EQE) depends on four parameters – charge carrier balance factor (γ), emission layer luminescence quantum efficiency (η_{RAD}), singlet and total excitons ratio ($\eta_{S/T}$), and output efficiency (η_{OUT}). These parameters are related by the following equation:

$$EQE = \gamma \cdot \eta_{S/T} \cdot \eta_{RAD} \cdot \eta_{OUT} \quad (1.16)$$

The fluorescence quantum efficiency of the emission layer depends on structures of the functional molecules and their film-forming properties. It is important to ensure that intermolecular interactions in the solid layer would be as small as possible, because it allows to ensure low fluorescence concentration quenching, which is key the reason for the low fluorescence quantum efficiency in the solid layer. Ratio between singlet and triplet excitons is determined by the structure of the molecule. As mentioned earlier, in case of traditional fluorescent emitters, only 25% of the excitons which were injected from the electrodes becomes singlets, so the ratio $\eta_{S/T}$, in this case, is ¼. In case of phosphorescent and TADF emitters, for the reasons discussed above, this ratio can reach up to 1. The other two parameters depend on the structure of the OLED. Charge carrier balance factor in an optimized OLED usually reaches 1. In case of low charge carrier balance factor, the turn-on voltage of the OLED usually is quite high which creates high operating voltages and low efficiencies as the result. The output efficiency factor shows how many of created photons leaves the device. When the light travels outside from the EML, complete internal reflections on the ITO-glass, glass-air and organic-ITO surfaces are created. The output efficiency coefficient for OLEDs of the standard structure (see Fig. 1.13) is around 0.2. η_{OUT} factor can be described by Snell's law simplification [60]:

$$\eta_{OUT} = \frac{1}{2n_{glass}^2} \approx 0.2. \quad (1.17)$$

Where n_{glass} is refractive index of glass. This coefficient can significant increase with molecular orientation when the output efficiency coefficient is close to 0.4 [61]. For a long time, molecular orientation has only been applied to the evaporation of OLEDs, however, there are some works which apply molecules orientation during OLEDs fabrication by spin-coating [62]. Multiplication of these four parameters (1 - ¼) × 1 × 1 × 0.2 is equal to 0.05 to 0.2. Which means that EQE of OLED with conventional fluorescence emitter is likely to be bellow 5% while EQE of the OLED with phosphorescent or TADF emitter can reach up 20%. Visual representation of OLED efficiency calculations can be seen in Fig. 1.14.

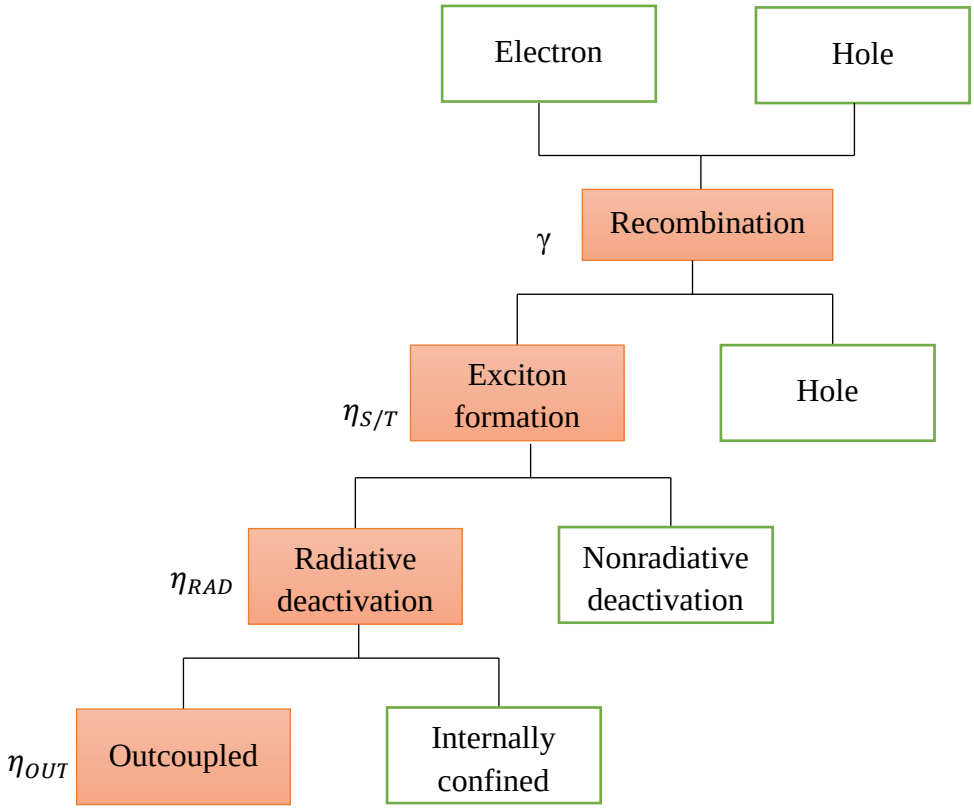

Fig. 1.14 Basic mechanism of OLED emission

As we can see charge carrier balance factor and singlet to total excitons ratio already reaches 1, so there are two main parameters that further improvements are needed to increase the EQE performance of OLEDs. Outcoupling efficiency, which can be successfully improved by the formation of photonic structures or orientation of the molecules will not be in the scope of this work. However, development of emission layers with high luminescence quantum efficiency is another way to make future progress in OLEDs fabrication. The aim of this work is to demonstrate the potential of novel hyperfluorescence structures as EMLs in OLEDs' technology field. In order to do that four novel organic semiconductors were synthesized. However, to successfully use them in fabrication of devices it is crucial to understand the nature of all four compounds. Because of that all new compounds have to be investigated using techniques which are described in the next section in order to characterize their photophysical and other functional properties before they can be used in the OLEDs. Finally, based on these results unique structures of OLEDs will be created in order to get optimal performance of devices.

2. Materials and research methods

2.1. Materials

The chemical structures of the studied mono and tetra phenothiazine substituted tetraphenylethylenes **PTZ-TPE-1, PTZ-TPE-2, PTZ-TPE-3** and **PTZ-TPE-4** are presented in Fig. 2.1. These compounds were recently designed and synthesized by our scientific partners from Chemistry department of Indian Institute of Technology Indore. Compounds **PTZ-TPE-1** and **PTZ-TPE-4** were synthesized by the Suzuki cross-coupling reactions between phenothiazine boronate ester with bromo tetraphenylethylenes while **PTZ-TPE-2** and **PTZ-TPE-3** were made by the Suzuki cross-coupling reactions between 4-(1,2,2-triphenylvinyl)-phenylboronic acid pinacol ester with 7-bromo-10-propyl-10H-phenothiazine-3-carbonitrile or 3-(7-bromo-10-propyl-10H-phenothiazin-3-yl)-2-phenylacrylonitrile, respectively. Cyano groups were attached at different positions of the phenothiazine core in order to demonstrate influence of electron-accepting group position while different number of phenothiazine moieties should show influence of twisting in the molecules which can affect photophysical properties of the compounds.

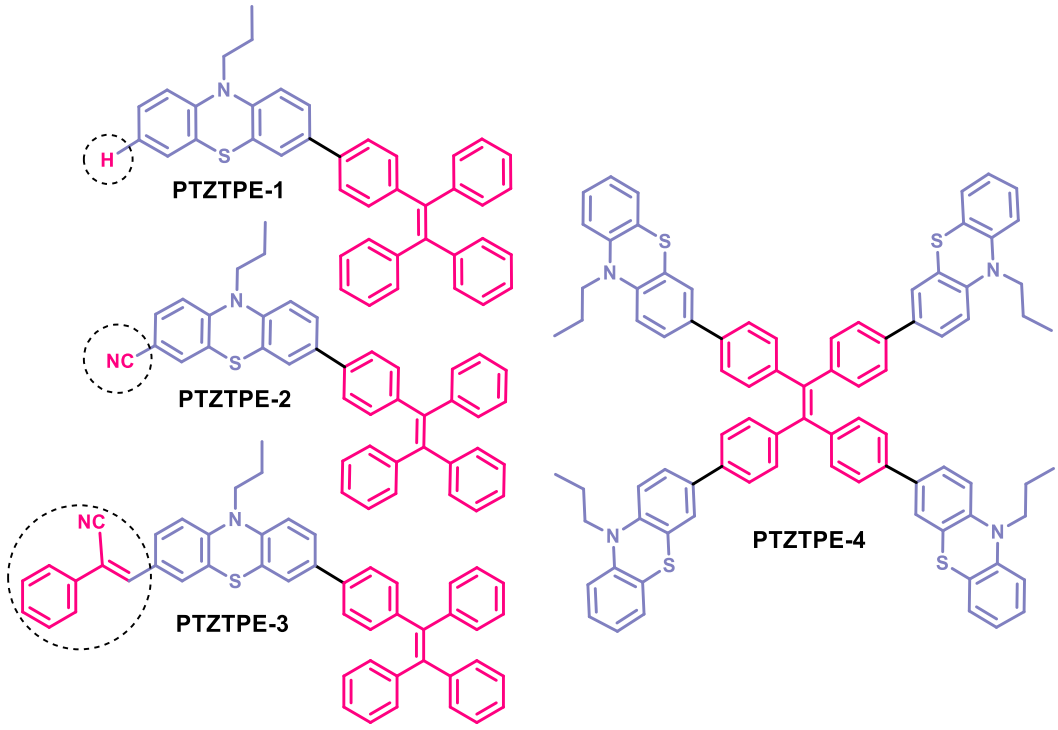

Fig. 2.1 Chemical structures of studied compounds

Other materials: 4,4',4''-Tris(carbazol-9-yl)triphenylamine (TCTA), N,N′-Di(1-naphthyl)-N,N′-diphenyl-(1,1′-biphenyl)-4,4′-diamine (NPB), 4,4′-cyclohexylidenebis[N,N-bis(4-methylphenyl)benzenamine] (TAPC), Poly(9,9-dioctylfluorene-alt-N-(4-sec-butylphenyl)-diphenylamine) (TFB), 1,3-bis(9-carbazolyl)benzene (mCP), diphenyl-4-triphenylsilyl-phenylphosphineoxide (TSPO1), 4,4'-(9H,9'H-[3,3'-bicarbazole]-9,9'-diyl)bis(3-(trifluoromethyl)benzonitrile) (pCNBCz0CF3), 1,4,5,8,9,11-Hexaazatriphenylenehexacarbonitrile (HAT-CN) and 2,2',2''-(1,3,5-benzinetriyl)-tris(1-phenyl-1-H-benzimi-dazole) (TPBi) were used as received from Sigma-Aldrich and LUMTEC companies for OLEDs fabrication. The chemical structures of these compounds can be found in Fig. 2.2.

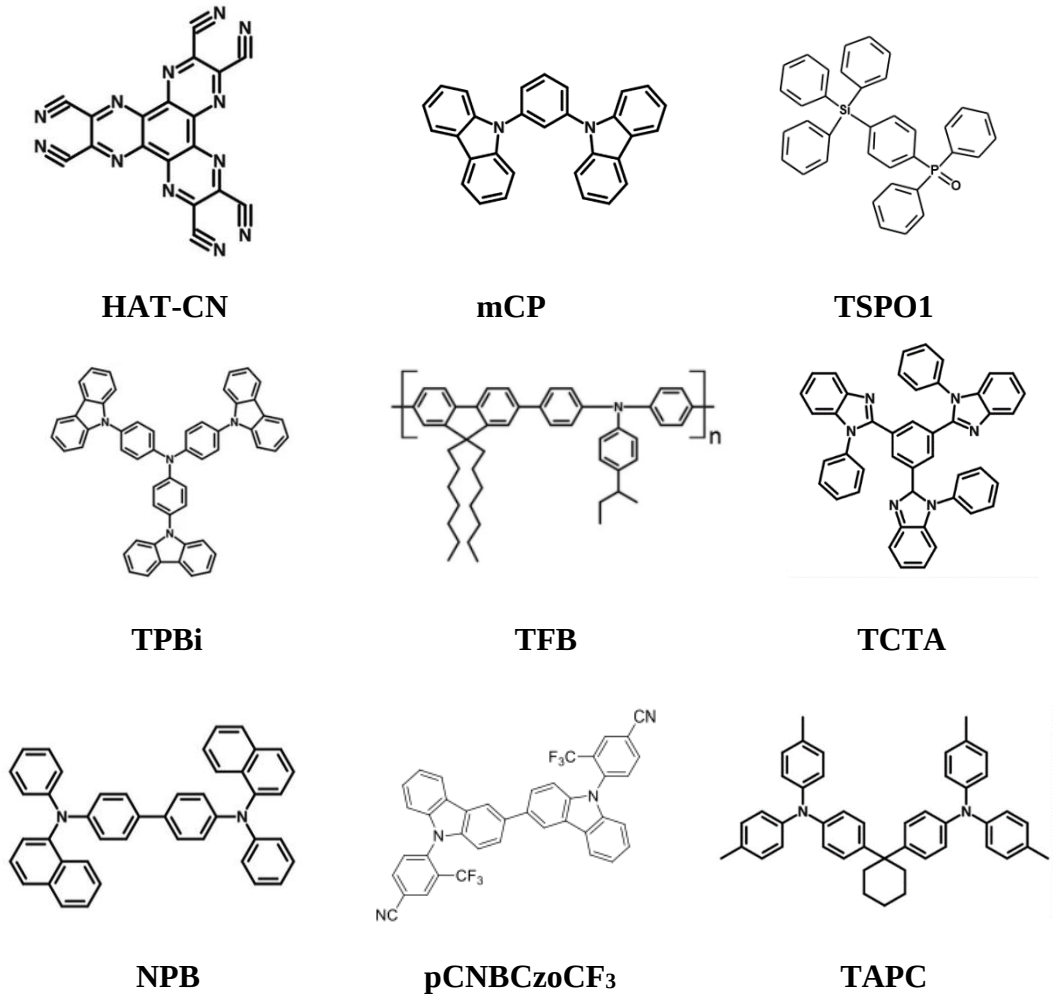

Fig. 2.2 Structures of chemical compounds which were used in the study

2.2. Instrumentation

An Edinburgh Instruments FLS980 spectrometer was used to record steady-state PL spectra of films (Fig. 2.3.). The FLS980 is fitted with a PicoQuant LDH-D-C-375 laser (wavelength 374 nm) as the excitation source for recording photoluminescence decay curves. The integrated sphere system was used to calculate the films' photoluminescence quantum yields (PLQY) (accuracy ±5%). (Fig. 2. 4).

Photoelectron emission spectrometry in air was used to determine the solid-state sample's ionization potential. A deep UV deuterium light source ASBN-D130-CM, a CM110 1/8m monochromator, and a Keithley electrometer 6517B were used during this experiment. The time of flight (ToF) method was used to calculate the charge carrier mobility (μ) of the vacuum deposited layers. A method of carrier extraction in linearly increasing voltage (CELIV) was used to determine the layer thickness. A pulsed Nd:YAG laser (EKSPLA NL300, wavelength 355 nm, pulse duration 3-6 ns), a Keithley 6517B electrometer, and a Tektronix TDS 3052C oscilloscope were used in the TOF experiment.

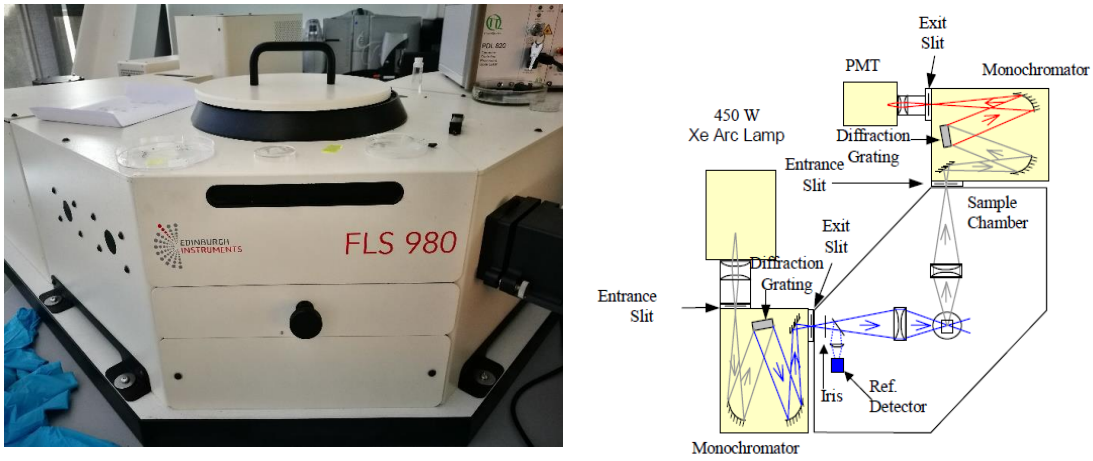

Fig. 2.3 "Edinburgh Instruments FLS980" spectrometer

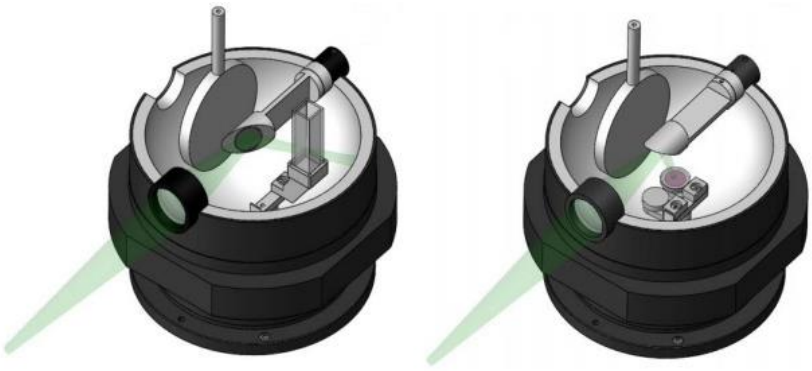

Fig. 2.4. a) Integrating sphare configuration in order to measure PLQY of liquids, b) confifuration of integrating sphare in order to measure PLQY of bulk, powder, film samples.

The current density-voltage and luminance-voltage characteristics of the fabricated devices were simultaneously recorded using the Keithley 2400C sourcemeter and the certificated photodiode PH100-Si-HA-D0 together with the PCBased Power and Energy Monitor 11S-LINK in air without passivation immediately after taking out of the samples from inert atmosphere. Electroluminescence (EL) spectra were taken by an Aventes AvaSpec-2048XL spectrometer. External quantum efficiency was calculated from the luminance, current density, and EL spectrum. The chromaticity coordinates (x, y) of the devices were calculated using EL spectra.

2.3. Preparation of samples

All phenothiazine substituted tetraphenylethylene derivatives were studied in three in different media – in diluted sulutions (10-6 -10-5 M), pure films and guest:host systems' films with different concentrations of the test substance. The first step in the preparation of the samples was their weighing and preparation of the concentrated solutions (10-3 - 5 × 10-3 M). The required volume of concentrate was then pour into 2.5 ml of THF solvent (standard medium polar solvent which was used to measure diluted solutions) in quartz cuvettes (which do not absorb UV) in order to make a dilute solution. Studied compounds layers were prapared by pouring the concentrate on quartz glass (2 cm x 2 cm) and evaporation of the solvent. Tetraphenylethylene concentration effects for their photophysical properties were studied by incorporating these compounds into mCP matrix. Concentrate solution in toluene was mixed in some ratio with mCP which was dissolved in toluene too. The resulting solution

was poured dropwise on the quartz substrate which was then left in fume cupboard to evaporate the solvent. After evaporation of the solvent, on a thin layer of test substance formed on the glass substrate. All procedures were done in the air.

Samples for TOF and ionization potencial measurements were prepared by vacuum deposition of organic and metal layers onto pre-cleaned ITO coated glass substrate under pressure lower than 2×10−6 mBar. The substrates were pre cleaned in acetone and isopropyl alcohol ultrasonic baths during ca. 10 min and by UV treatment during 15 min before deposition of the layers.

2.4. Measurements of spectra and lifetimes of photoluminiscence

For the excitation of steady fluorescence of the studied compounds a 150 W xenon lamp with the spectral bandwidth up to 10 nm was used. The desired wavelength of light was separated by monochromator. In order to cut the shortwave slope of the lamp emission spectrum so it would not deform fluorescence signal, a suitable filter was used. Fluorescence spectra of the samples were collected via quartz fiber and recorded by CCD spectrometer with software which includes spectral sensitivity correction curve. When measuring fluorescence spectra, fiber was built perpendicular to the direction of light propagation.

The fluorescence lifetimes of the solutions and thin films were measured using the time-correlated single photon count method. The PicoQuant LDH-D-C-375 laser equipped to the FLS980 spectrometer was used for the studies. Fluorescence kinetics measurement starts with a short pulse semiconductor laser (374 nm) which excites the sample and activates the timer (see Fig. 2.5). The lens focuses the light flux into the sample. The photons which were emitted from the sample are collected and reconstituted into parallel fiber. This fiber is then focused into a monochromator, so the signal entering the monochromator is only fluorescent photons. The monochromator extracts the wavelength which is investigated, from which the signal enters detector.

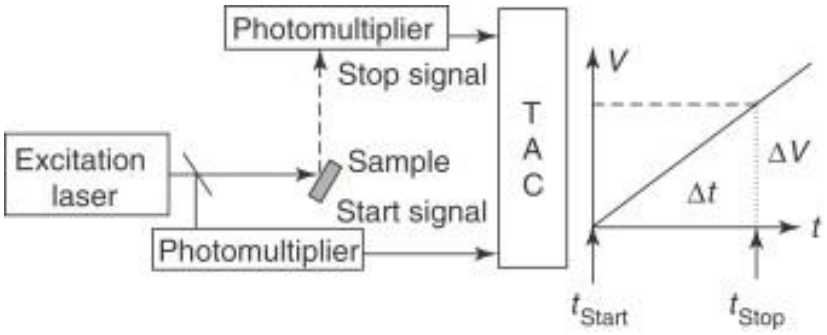

Fig. 2.5 Shceme for time-correlated photon count for fluorescence lifetime measurements

Time-correlated photon count is a measurement technology that calculates photons correlated according to the time elapsed since the moment of excitation. The method is based on a converter changing the time to a voltage amplitude that can be perceived as very fast stopwatch. Once the stopwatch is started excitation laser light, the voltage in the pulse converter starts to increase steadily (see Fig. 2.5). The voltage rises linearly until the first fluorescence photon is captured, which stops this growth. The voltage value is transmitted to a multichannel analyzer, which distributes the received data into channels, summing the results in each of the channels and the obtained results are presented as a function of the number of photons over time. The experiment is continued until a

"peak" channel of the histogram reaches about 10,000 photons. Thus, this histogram shows the fluorescence intensity of the sample evolution over time.

2.5. Photoluminescence quantum yield measurements

PLQY is a parameter that expresses the efficiency of a compound's emission as a ratio of emitted photons to photons that were absorbed. In order to calculate the PLQY integrating sphere whose inner cavity is covered with a highly reflective material (barium sulfate (Ba2SO4)) was used. PLQY evaluation requires the precise measurement of the emission spectrum and the measurement of the absorbed number of photons. Two emission scans are used to perform the measurement, with the emission monochromator scanning over the Rayleigh scattered light from the sample and a 100% diffuse reflecting reference. It should be noted that precise spectral correction is essential for the PLQY calculations. However, data should be recorded by simultaneous detection of the signal without spectral correction taking into account spectral function of the emission channel. This correction should be applied to the raw data after background subtraction only after the measurement is done. After that the PLQY is calculated using aF980 software wizard and spectrally corrected curves. Figure 2.6 shows two spectral scans obtained by scanning the emission monochromator while keeping the excitation monochromator at 450nm. The first scan (blue) is of a reference scatterer, which should have 100 percent diffuse reflectance. The sample under examination is scanned in the second scan (red). This example shows both emission (red, solid) and reflection(red, hatched). The blue graph's region (starting at the base line) is called E_{Ref}, the red hatched area is called E_{Sam}, and the red solid area is called L_{Sam}.

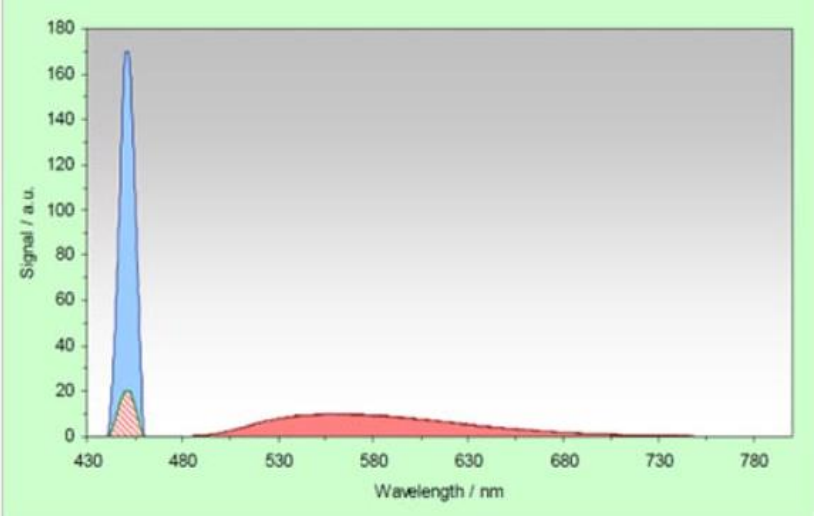

Fig. 2.6 Graphical representation of specta for PLQY calculations [62]

Then PLQY can be calculated by the following equation:

$$PLQY = \frac{L_{Sam}}{E_{Ref} - E_{Sam}} \cdot 100\% \quad (2.1)$$

It should be remembered that according to the supplier this absolute method for measuring the PLQY has an average error of 5%, assuming no systematic error exists, while repeatability is accurate to within 3%. Count rate saturation and incorrectness of the data file used for spectral correction of the raw data are two main potential sources of systemic errors [63].

2.6. Testing of aggregation induced emission phenomenon

AIE/AIEE properties of the studied mono and tetra phenothiazine substituted tetraphenylethylenes were tested by comparing their fluorescence spectra and intensity in pure THF solutions versus fluorescence spectra and intensity in THF/H_2O mixtures containing different water fraction. Since these tetraphenylethylene derivatives easily dissolve in THF, but do not dissolve in water, increasing water fraction in the THF/H_2O mixture will result in studied molecules transformation into nano-aggregate particles. After formation of these aggregates, motion of the molecules will be restricted what will allow to test AIE/AIEE properties of the compounds. The following steps were done in order to perform the measurement:

1. Weighted needed amount of studied compouds;
2. A concentrate THF solutions of $2 \cdot 10^{-4}$ M **PTZ-TPE-1/PTZ-TPE-2/PTZ-TPE-3/PTZ-TPE-4** were prepared;
3. An equal amounts (20μl) of the concentrate solution were transferred to the separate quartz containers;
4. Concentrate solutions which were in containers were diluted with THF – 80, 180, 280, 380, 580, 780, 980, 1180, 1380, 1580, 1780, 1980μl of THF was added into individual containers;
5. A distilled water was added to the solution. Dilution was performed dropwise with vigorous stirring, so the total volume of each solution would be equal to 2ml;
6. After solutions were prepared, they were transferred to a 3.5 mL quartz cuvettes.
7. After that, measurements of the photoluminescence spectra of the resulting solutions were carried out immediately after their preparation.

2.7. Ionization potential measurements

The ionization potential (I_P) indicates what energy E_{th} is needed for an electron to be released outsidse from the material. The following steps were done in order to perform the measurement:

1. Pre clean substrates in acetone and isopropyl alcohol ultrasonic baths;
2. Treat substrate in ozone atmosphere for 10min;
3. Prepare solution of the test substance in THF;
4. Prepared solution is poured dropwise on the substrate;
5. Susbstrate with the layer of studied compound is anealed for 10min at 60 °C temperature;
6. Negative voltage is applied to the substrade while another electrode is placed 3mm away from the layer of the studied compound;
7. Sample illuminated by monochromaric light created by deep UV deuterium light source ASBN-D130-CM and CM110 1/8 m monochromator;
8. Energy of incident light is being linearly increased;
9. The generated photocurrent is written by the following equation:

$$I^{0.5} = A(h\nu - E_{th}) \tag{2.2}$$

where A is the electron work-function and E_{th} is the threshold of the external photo effect

10. Created photo-current is measured by 6517B Keithley electrometer;
11. The obtained results are represented in the Cartesian coordinate system and linearly approximated to the intersection with the axis of the abscissa. The intersection point corresponds to the ionization potential.

More information about such measurement can be found in the article ” Dynamics of fluorescence depolarisation in star-shaped oligofluorene- truxene molecules“ [64].

2.8. Time-of-flight measurement

The charge carrier mobility is one of the most important performance parameters of an organic semiconductor. In this study charge mobilities were measured using time-of-flight (ToF) technique [65] basic setup of which is visualized in Fig. 2.7. The following steps were done in order to perform the measurement:

1. Pre clean substrates with ITO electorde in acetone and isopropyl alcohol ultrasonic baths;
2. Treat substrate in ozone atmosphere for 10min;
3. Using vacuum deposition prepare sandwich-like samples (ITO/PTZ-TPE-1, PTZ-TPE-2, PTZ-TPE-3, PTZ-TPE-4/Al). During the deposition vacuum higher than $2 \cdot 10^{-6}$ mBar was employed. The thickness of organic PTZ-TPE-1, PTZ-TPE-2, PTZ-TPE-3, PTZ-TPE-4 layers were 1.3, 2.9, 2.6 and 2.5 μm respectively which were controlled via quartz resonator;
4. Sample was iluminated by Nd:YAG laser (EKSPLA NL300) with a 355 nm wavelength and 3–6 ns pulse width;
5. Multiple different external voltages were applied to the sample via a 6517B Keithley electrometer.
6. Under each voltage resulting photocurrent was evaluated by a Tektronix TDS 3032C digital oscilloscope.
7. Charge mobilities were evaluated using following equation:

$$\mu = \frac{d^2}{U \cdot t_{tr}} \tag{2.3}$$

where U is applied voltage, t_{tr} – a transit time and d – thickness of layer.

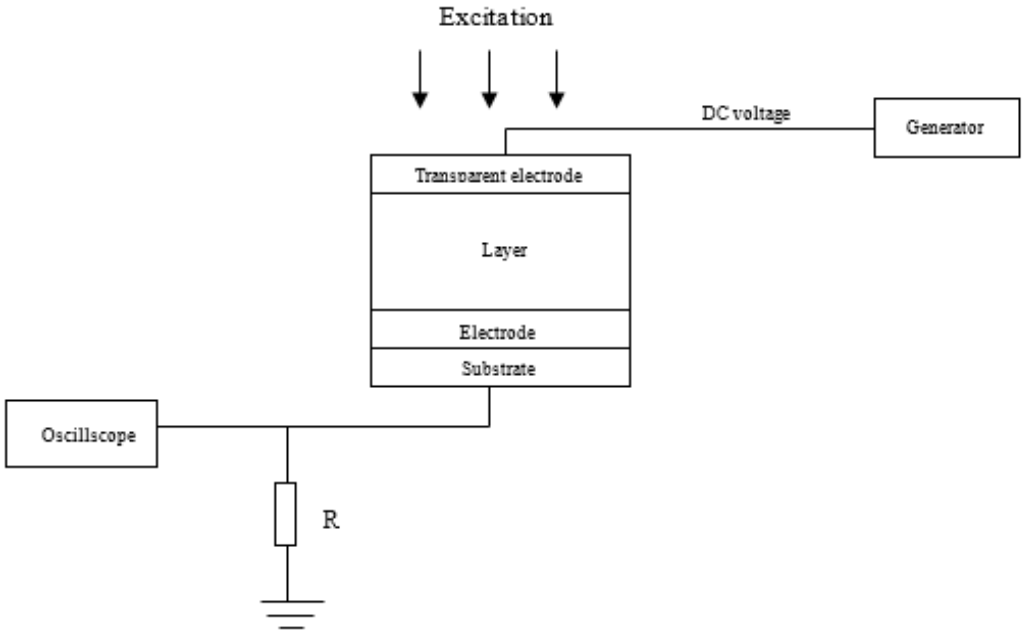

Fig. 2.7 Scheme of Time-of-flight measurement

2.9. Measurement of layer thickness

The layer thickness measurements of the samples were performed using Charge Extraction by Linearly Increasing Voltage method. Schematic of measurement setup can be seen in Fig. 2.8.

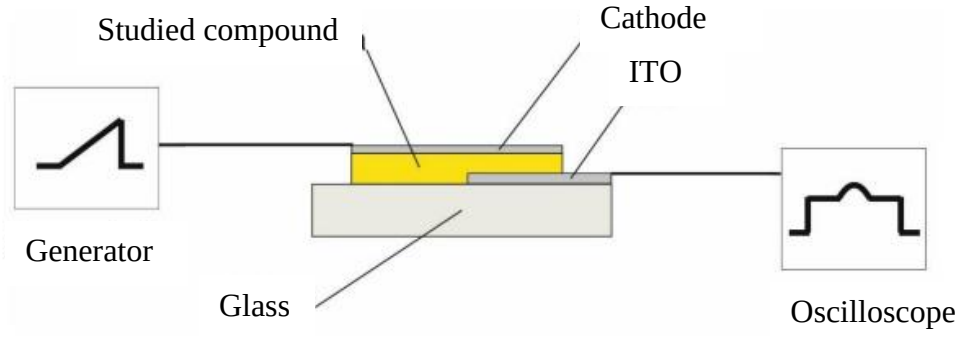

Fig. 2.8 Schematic measurement scheme of the investigated layer

The following steps were done in order to perform the measurement:

1. Connect the sample to the measurement circuit in the reverse direction (cathode to the generator and ITO to the oscilloscope);
2. Adjust and prepare generator and oscilloscope for the work. Set generator and supply a triangular voltage signal as shown in Fig. 2.8;
3. On the oscilloscope screen we need to see the response of the sample to the transmitted signal (function under voltage);
4. Write down the voltage of the sample recorded on the oscilloscope display;
5. Calculate the thickness of the sample:

   – Charge accumulated in the sample equal to:

   $$Q = C_b \cdot U \tag{2.4}$$

   whre C_b is the capacity of the sample.

   – Rate of voltage change equal to:

   $$A = \frac{U}{t} \tag{2.5}$$

   – Next, we enter formula (2.4) in the expression of current:

   $$I = \frac{dQ}{dt} = \frac{d(C_b \cdot U)}{dt} = U\frac{dC_b}{dt} + C_b\frac{dU}{dt} \tag{2.6}$$

   – Since the capacity of the sample does not change, the first term of equation (2.6) is equal to 0, and the second term we simplify by using formula (2.5), then:

   $$I = C_b \cdot A \tag{2.7}$$

   – Compare expression of current (2.7) with Ohm's law:

   $$I = \frac{U}{R} = C_b \cdot A \tag{2.8}$$

   – From formula (2.8), we express the capacity C_b and introduce it into the formula of the flat capacitor capacity:

   $$C_b = \frac{\varepsilon\varepsilon_0 S}{d} = \frac{UA}{R} \tag{2.9}$$

   – From formula (2.9) we express the thickness d of the sample:

   $$d = \frac{\varepsilon\varepsilon_0 SAR}{U} \tag{2.10}$$

2.10. Preparation of the devices

Substrate preparation and application of appropriate layer forming technologies are important factors and have strong influence on produced OLEDs characteristics, so it is important to ensure consistency of production and cleanliness throughout the whole process. Dust or other dirt can damage the structure of the device and have negative influence on its performance.

– Preparation of the substrate:

1. Firstly, the quartz substrates are cleaned with acetone. This solvent reacts with organic substances and other impurities by dissolving them. However, this cleaning does not remove all dirt;
2. After that substrates were cleaned in distilled water, acetone and isopropyl alcohol ultrasonic baths during ca. 10 min. Ultrasound removes dirt which is heavily stuck or even penetrated into the substrate.
3. Lastly, all substrates were treated by ozone for 15min. After all these procedures, the substrates are prepared for further preparation of the devices.

– Fabrication of layers by vacuum deposition:

1. First of all, before starting evaporation process it is also important to properly prepare hardware which is going to be used for work. It must be cleaned with acetone solvent as it has previously evaporated particles adhere to almost all the surfaces of the chamber. During new evaporation these particles can adhere to the new layer and change its electrical properties;
2. Pre-cleaned ITO-coated substrates with a sheet resistance of 15 Ω/sq which also were patterned to get seven independent structures placed to the chamber;
3. Studied compounds with a special spoon is placed in a glass crucible, and the crucible is inserted into a heating element formed of tungsten wire. The hood is closed. Schematic of the vacuum deposition chamber is demonstrated in Fig 2.9 [66];
4. Air is pumped from under the hood (1) with a rotary pump (2) (see Fig. 2.9 a) up to a certain limit (primary vacuum);
5. In order to create secondary vacuum, diffusion pump is switched on (3). Inside of the diffusion pump is filled with oil, which is heated and therefore requires cooling with water. We also leave a rotary pump working in order to pump air from the diffusion pump;
6. Under the hood is created vacuum higher than 2×10^{-6} mBar which is already suitable for the evaporation of organic matter;
7. The current source required to heat the tungsten wire is turned on and appropriate evaporating current that corresponds to a certain temperature is select. After tungsten wire is heated to the selected temperature, the evaporation process begins;
8. Evaporation speed can be monitored by display of vacuum equipment from Kurt J. Lesker which is built in an MB EcoVap4G glove box;
9. The same technology and hardware are used for cathode evaporation. The difference is that substrates are placed under the special mask with cut-out electrode shapes.

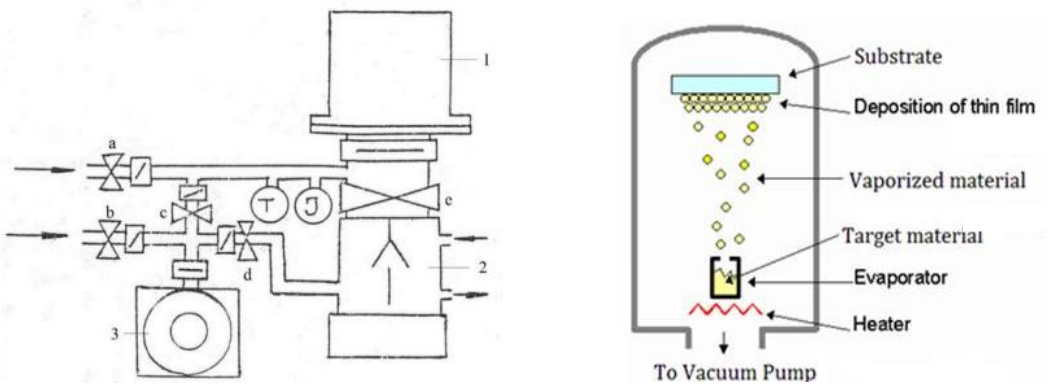

a) b)

Fig. 2.9 a) Schematic of the vacuum equipment: 1 - hood, after which materials are evaporated, 2 - diffusion pump, 3 - rotary pump, electromagnetic vacuum valves are marked a, b, c and d, b) Cross sectional view of an organic vacuum deposition system

– Fabrication of layers by spin-coating:

1. During spin coating studied compounds solution is is applied to the substrate which starts rotating. Mostly all solution is expelled from the substrate and only a thin layer of material remains on the surface. In that way the surface area of solution increases and the solvent evaporates rapidly. Layer thickness, morphology and surface topography can be successfully replicated if the concentration of solution is the same. These three properties of the layer are highly dependent on the rotation speed, solution viscosity, molecular weight, concentration and other its parameters;
2. The TBF layer was spin-coated using its 4 mg/ml solution and 1000rpm speed;
3. The EML containing three components co-hosts pCNBCz0CF3 and mCP and studied compounds as an emitters was spin-coated using their 5mg/ml solution and 1000rpm speed;
4. The fabricated layers were annealed for 30 minutes on the hot plate after each spin-coating procedure;
5. Temperatures of 150 °C and 70 °C were used for TFB and EML layers, respectively.

2.11. Determination of devices properties

If devices are being measured in the air, it is important to take measurements as soon as possible after removing the samples from an inert environment in such way preventing passivation.. The following steps were done in order to perform the measurement:

1. Connect the sample to the measuring circuit in a direct direction;
2. When a rectangular voltage pulse is applied to the sample, the injection of the carriers is started. Increasing voltage, the amount of charge carriers injected into the sample increases, which increases the likelihood of charge carriers recombining in radiative way, i. there will be a higher probability of electroluminescence;
3. The Keithley 2400C sourcemeter and the certificated photodiode PH100-Si-HA-D0, as well as the PCBased Power and Energy Monitor 11S-LINK, were used to simultaneously record the current density-voltage and luminance-voltage characteristics of the fabricated devices.
4. Electroluminescence spectra were taken by an Aventes AvaSpec-2048XL spectrometer;
5. The received data is processed by a computer;
6. EQE was calculated from the brightness, current density, and electroluminiscence spectrum;
7. Electroluminiscence spectra of the devices were used to calculate their chromaticity coordinates.

3. Research results and discussion

3.1. Photoelectrical and charge-transport properties

3.1.1. Electron photoemission spectrometry

One of the most important organic semoconductors‘ characteristics which can determine whatever their can be used in OLEDs is charge injection properties. Since all of the compounds under investigation will be used as solid films, their ionization potentials (I_p^{EP}) were calculated using electron photoemission spectroscopy (Fig. 3.1).Photocurrent versus photon energy (hv) plot showed that I_p^{EP} of the studied compounds varies between 5.48 eV and 5.63 eV. All values of I_p^{EP} are represented in Table 1. As expected, electron withdrawing group substitutions have a noticeable effect on charge-transporting energy levels of the studied tetraphenylethylenes derivatives. It is represented by the fact that compound **PTZ-TPE-1** which does not have a cyano group was characterized by the lowest I_p^{EP} in comparison with **PTZ-TPE-2** - **PTZ-TPE-4.** Koopmans' theorem states that I_p^{EP} of a molecule is opposite to the HOMO energy of that material. Therefore, HOMO energy levels of the studied compounds are equal to -5.48, -5.63, -5.56 and -5.59 eV.

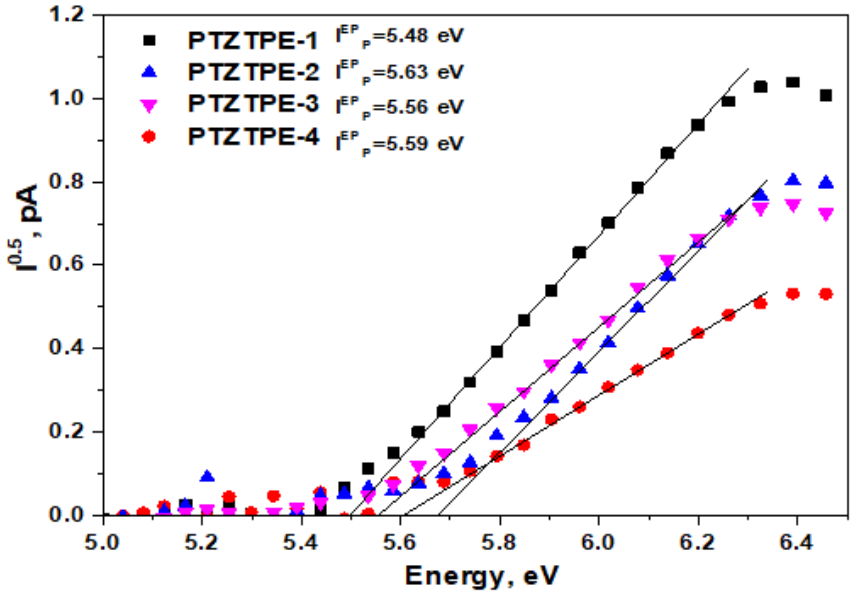

Fig. 3.1 Photoelectron spectra for vacuum-deposited films on the studied **PTZ-TPE-1-PTZ-TPE-4** compounds.

Having this data electron affinities (E_A^{EP}) of studied tetraphenylethylenes were calculated by using following equation

$$E_A^{EP} = I_P^{EP} - E_g \quad (3.1)$$

where E_g is the optical band-gap energy. The E_g values of **PTZ-TPE-1, PTZ-TPE-2, PTZ-TPE-3** and **PTZ-TPE-4**, were determined using Tauc plot of their pure solid-state films and are equal to 2.88, 2.73, 2.32 and 2.64 eV, respectively (see Fig. 3.2). Calculations showed that E_A^{EP} of the studied compounds varies between 2.6 eV and 3.24 eV. All values of E_A^{EP} are represented in Table 1. Since LUMO energy level is opposite to an E_A^{EP}, it was equal to -2.6, -2.9, -3.24 and -2.95 eV for **PTZ-TPE-1, PTZ-TPE-2, PTZTPE-3** and **PTZ-TPE-4**, respectively. Based on electron photoemission spectrometry results, it can be concluded that values of both I_P^{EP} and E_A^{EP} for all studied compounds

are in perfect ranges for hole and electron injection from electrodes of charge-transporting layers, respectively.

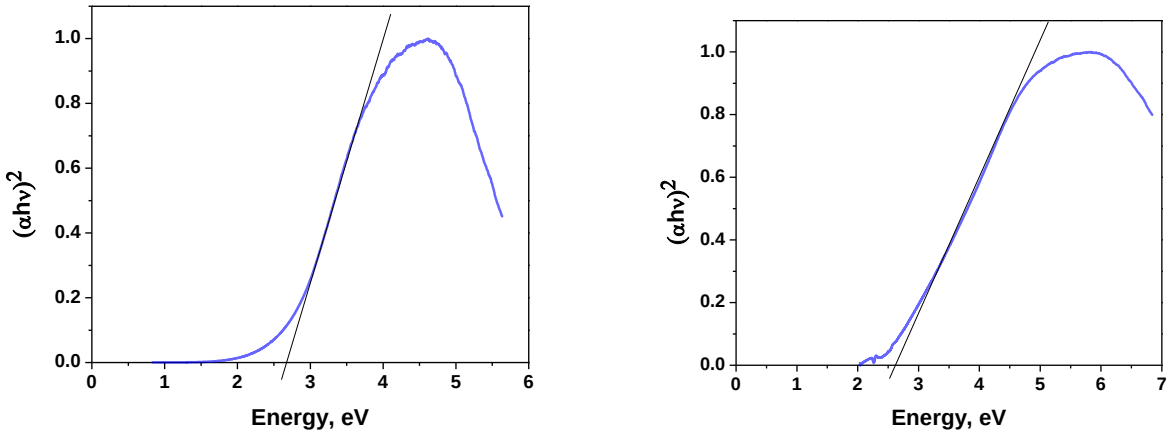

a) b)

Fig. 3.2 a) Tauc plot of **PTZ-TPE-2** vacuum deposited film, b) Tauc plot of **PTZ-TPE-4** vacuum deposited film

Table 2. Charge mobilities and energy levels for the vacuum-deposited studied compounds' layers.

Compound	PTZ-TPE-1	PTZ-TPE-2	PTZ-TPE-3	PTZ-TPE-4
μ_h ($cm^2 V^{-1} s^{-1}$)*	1.67×10^{-4}	6.5×10^{-6}	7.6×10^{-6}	4.7×10^{-6}
μ_0 ($cm^2 V^{-1} s^{-1}$)	4.2×10^{-6}	1.5×10^{-9}	3.3×10^{-9}	4.3×10^{-8}
α ($cm\ V^{-1})^{1/2}$	0.0055	0.009	0.0081	0.0069
I_p^{PESA} (eV)	5.48	5.63	5.56	5.59
E_g^{film} (eV)	2.88	2.73	2.32	2.64
E_a^{film} (eV)	2.6	2.9	3.24	2.95

*values recorded at electric field of 4.6×10^5 V/cm. μ_h is hole mobility. μ_0 is zero-field mobility, α is field dependence parameter.

3.1.2. Time-of-flight measurements

The charge-transporting properties of vacuum-deposited films were tested using the time-of-flight (TOF) technique in order to investigate the potential of the studied **PTZ-TPE-1** - **PTZ-TPE-4** compounds as semiconductors for various organic electronic applications. In order to accomplish this, TOF current transients were reported under both positive (for holes) and negative (for electrons) external (see Fig. 3.3). All TOF measurement are presented in Fig. 3.3, Fig 3.4 and Table 2. Transit times (t_{tr}) for holes can be well observed from corresponding TOF transients' shapes which allow to make conclusion about low dispersity of hole transport. However, in case of electrons no transit times were not obtained which means that studied compounds are only capable of transporting holes.

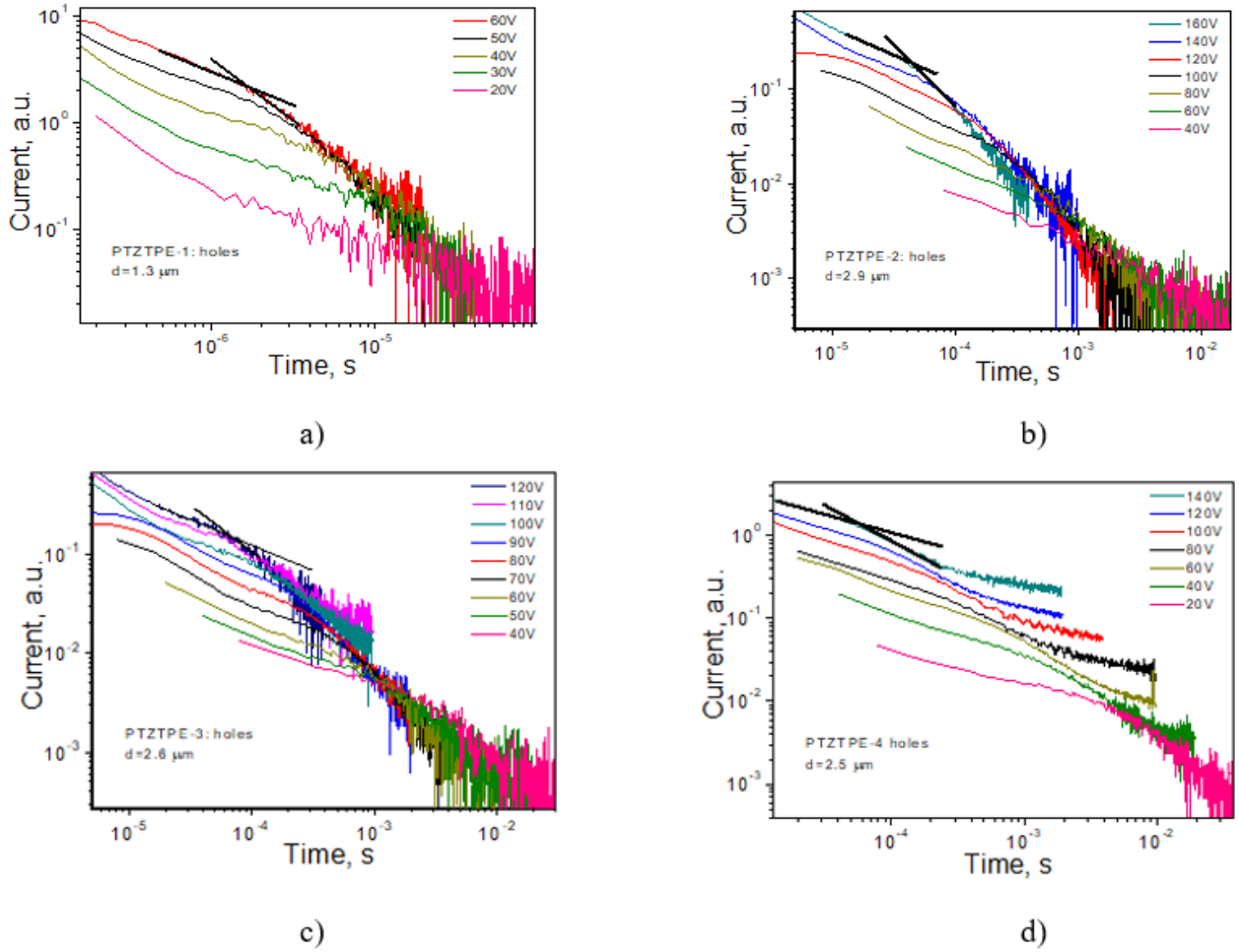

Fig. 3.3 TOF signals for holes of a) **PTZ-TPE-1** b) **PTZ-TPE-2**, c) **PTZ-TPE-3**, d) **PTZ-TPE-4** layers

Hole mobilities were determined using formula 2.3 and measured transit times for holes at various applied voltages. Calculated charge mobility dependencies on electric field are represented in Fig. 3.4. In case of compounds **PTZ-TPE-2**, **PTZ-TPE-3** and **PTZ-TPE-4** almost the same hole mobilities of 4.7-7.6×10^{-6} cm^2/Vs at electric field of 4.6×10^5 V/cm were obtained. It means that electron withdrawing group substitutions do not have significant influence on charge mobility of the studied compounds. The non-planar molecular structures of compounds **PTZ-TPE-2**, **PTZ-TPE-3** and **PTZ-TPE-4**, which prevent near molecular packing in the solid state, clarify the low hole mobilities. Since Poole–Frenkel type charge mobility can be calculated by a relationship

$$\mu = \mu_0 e^{\alpha E^{1/2}} \tag{3.2}$$

where α is field dependence parameter, different α of the compounds results in relatively large range of in their zero-field mobility – 1.5 - 4.3× 10^{-9} cm^2/Vs. All field dependence parameters and zero-field mobilities can be found in table 2. In case of compound **PTZ-TPE-1** charge mobility under the same 4.6×10^5 V/cm electric field was several magnitudes higher and equal to 1.67×10^{-4} cm^2/Vs. Different molecular packing in solid film of **PTZ-TPE-1** results in more suitable HOMO-HOMO overlapping for hole hopping between neighboring molecules, which can explain the disparity of charge mobility between **PTZ-TPE-1** and the rest of the compounds. Overall, charge mobility measurement results show potential of studied phenothiazine substituted tetraphenylethylenes to be

used as emitters in OLEDs but not as charge-transporting materials or hosts because even their hole mobilities are much lower than hole mobility values of efficient hole-transporting materials [67].

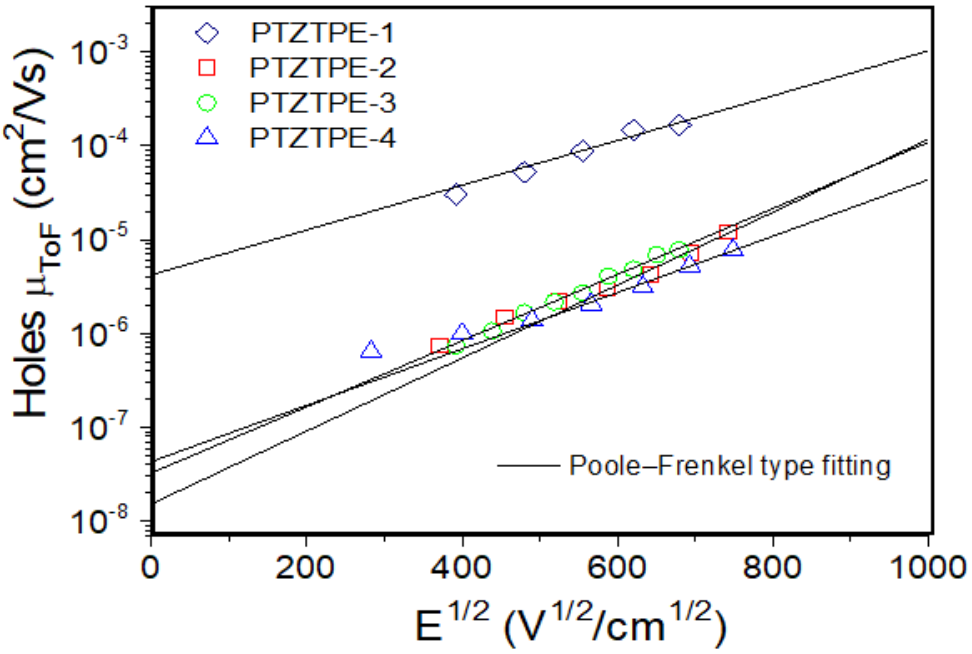

Fig. 3.4 Studied compounds holes mobilities versus electric fields

3.2. Photophysical characterizations

3.2.1. Absorption and Photoluminescence

Investigation of studied mono and tetra phenothiazine substituted tetraphenylethylenes **PTZ-TPE-1, PTZ-TPE-2, PTZ-TPE-3** and **PTZ-TPE-4** photophysical properties were started from characterization of their absorption and emission spectra in dilute solutions. The electronic absorption and emission spectra of all studied compounds are visualized in Fig. 3.5 and the related data are illustrated in Table 3. The absorption spectra of **PTZ-TPE-1, PTZ-TPE-2, PTZ-TPE-3** and **PTZ-TPE-4** in THF solvent (10^{-5} M) demonstrate a sharp absorption band in shorter wavelength region at 274nm, 280 nm, 304 nm and 270 respectively, which is related to the π-π* transitions while peaks in longer wavelength region observed at 323 nm, 322 nm, 423 nm, 355 nm for **PTZ-TPE-1, PTZ-TPE-2, PTZ-TPE-3** and **PTZ-TPE-4,** respectively, can be attributed to charge transfer (CT) bands. CT related peaks in longer wavelength region can be caused by D-A character generated in the molecules, however to confirm this solvatochromism measurements will have to be performed. Tetraphenylethylenes derivatives are normally non-emissive in solution due to non-radiative energy loss of excited states caused by the free rotation of the phenyl rings of tetraphenylethylenes. However, due to electron withdrawing moieties, studied compounds **PTZ-TPE-1** – **PTZTPE-4** are emissive even in solutions. The **PTZ-TPE-1** demonstrates chartreuse colored emission (λ_{em} =539 nm) with a Stokes shift of 12407 $cm^{-}1$, **PTZTPE-2** shows an intense cyan colored emission (λ_{em} =482 nm) with a large stokes shift of 10309 cm^{-1}, **PTZ-TPE-3** was characterized by yellow colored emission (λ_{em} =585 nm) with a stokes shift of 6547 cm^{-1}, while **PTZ-TPE-4** shows yellowish colored emission (λ_{em} =574 nm) with a stokes shift of 10747 cm^{-1} (see Fig. 3.5).

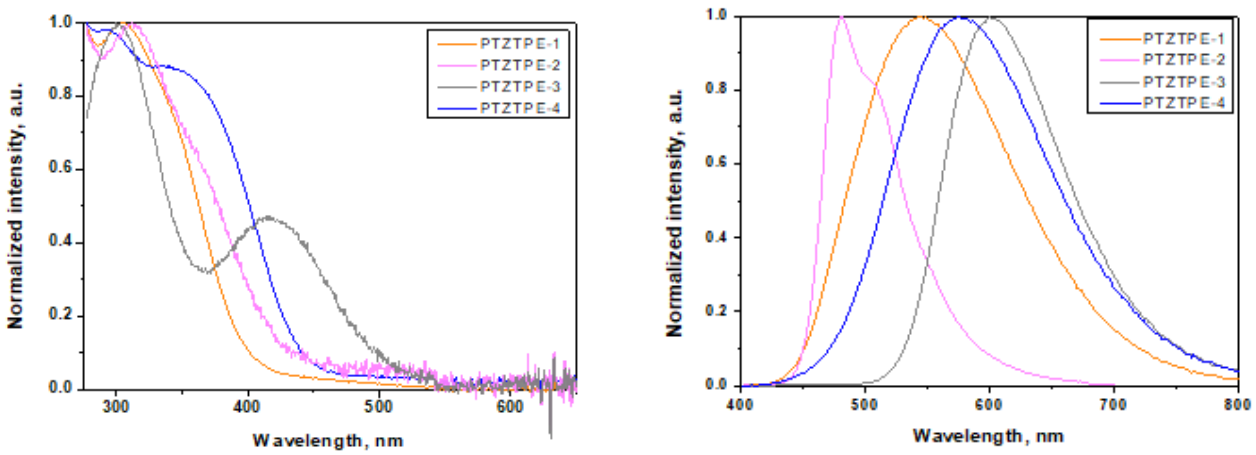

Fig. 3.5 (a) Absorption and (b) normalized emission spectra of studied compounds in THF solvent (10^{-5} M) (Excitation wavelength λ_{exc} = 350 nm)

Non-deoxygenated dilute solutions of **PTZ-TPE-1, PTZ-TPE-2, PTZ-TPE-3** and **PTZ-TPE-4** in toluene showed PLQY values equal to 3.2, 29.8, 66 and 5.8% respectively. After deoxygenation of the samples PLQY values remained almost the same what indicates that emission with an origin in a triplet state does not have a major role in fluorescence mechanism of the studied compounds. PLQY values of pure **PTZ-TPE-1, PTZ-TPE-2, PTZ-TPE-3** and **PTZ-TPE-4** films were equal to 23.9, 27.6, 28 and 19.3%, respectively. In case of **PTZ-TPE-1** and **PTZ-TPE-3** PLQY values increased after films were doped in mCP which is normally expected because in this case ACQ influence become smaller. However, in case of **PTZ-TPE-2** and **PTZ-TPE-4** PLQY values of mCP doped films is lower that of the pure films (see Table 3) what indicates presence of AIE or AIEE effects.

Table 3. Photophysical properties of the studied compounds.

Compounds	λ_{abs} (nm), ε ($Lmol^{-1}cm^{-1}$)[a]	λ_{em} (nm)[a]	Stokes shift (cm^{-1})	Φ_f[b]	Φ_f[c]	Φ_f[d]
PTZ-TPE-1	274 (17700), 323 (8620)	539	12407	0.239	0.304	0.032
PTZ-TPE-2	280 (50590), 322 (23350)	482	10309	0.276	0.243	0.298
PTZ-TPE-3	304 (30230), 423 (10250)	585	6547	0.280	0.387	0.660
PTZ-TPE-4	270 (24940), 310 (15470), 355 (13090)	574	10747	0.193	0.170	0.058

[a] Recorded in dry THF (10^{-5} M concentration). [b] PLQY of pure films, [c] PLQY of films doped in mCP, [d] PLQY of toluene solutions (10^{-5} M concentration).

Due to the fact that studied compounds will be used as solid functional layers in OLEDs, PL spectra in solid state were investigated. All PL spectra and time decays are shown in Fig 3.6. Pure solid-state samples of **PTZ-TPE-1, PTZ-TPE-2, PTZ-TPE-3** and **PTZ-TPE-4** showed emission maxima at 473, 464, 575 and 506 nm, respectively. PL of the films of 15 wt% **PTZ-TPE-1, PTZ-TPE-2, PTZ-TPE-3** and **PTZ-TPE-4** hosted by mCP in all cases showed red-shifted emission maxima at 505, 485, 596 and 558 nm, respectively, which were similar to the values of dilute THF solutions. However, doping had almost no influence on PL decay times of studied phenothiazine substituted tetraphenylethylene derivatives (see Fig. 3.6). It means that the origin and mechanism of PL are unaffected by concentration, while variations in PL maxima can be explained by aggregation or solvatochromic-like effects due to differences in dielectric constants between the solvents, emitters, and hosts used during the experiment.

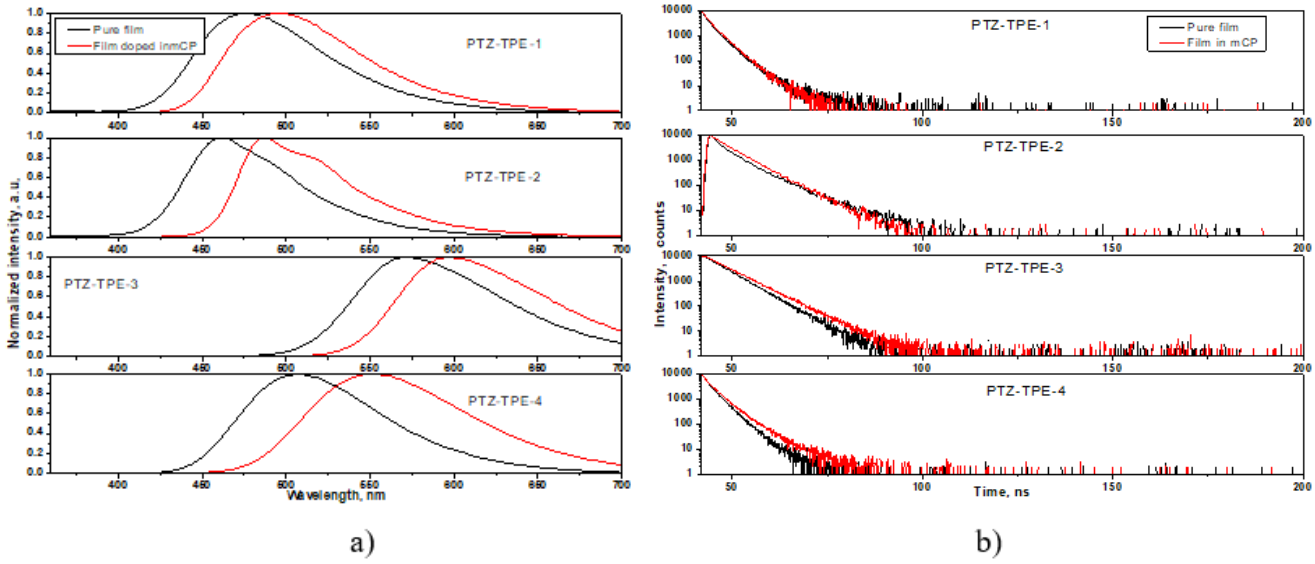

Fig. 3.6 a) PL spectra and b) time decays of **PTZ-TPE-1, PTZ-TPE-2, PTZ-TPE-3** and **PTZ-TPE-4** pure and mCP doped films

3.2.2. Solvatochromism

In order to examine CT nature of absorption peak solvatochromism measurements with different organic solvents (toluene, 1,4dioxane, tetrahydrofuran, dichloromethane and N,N-dimethylformamide) were performed. Influence of different polarity surroundings on **PTZ-TPE-2** and **PTZ-TPE-3** absorption and emission spectra is presented in Fig. 3.7. In case of absorption spectra, different polarity of the solvents does not show much influence on behavior of studied compounds. However, emission spectra demonstrate noticeable bathochromic shifts which indicate the D-A characteristics of the studied tetraphenylethylene. It can be explained in a way that excited states usually are more polar in comparison with the ground states. Because of that polar solvents stabilize the excited states more than the ground states resulting in the energy decrease of excited states. In non-polar solvents like toluene, the emission peaks of **PTZ-TPE-1, PTZ-TPE-2, PTZ-TPE-3** and **PTZ-TPE-4** were observed at 459 nm (sky blue), 480 nm (blue), 563 nm (yellow) and 564 nm (yellow), respectively. As mentioned before under increase of polarity, emission spectra show bathochromic shift and in polar solvents like DMF the emission maxima was at 631 nm (red), 492 nm (cyan), 613 nm (red) and 580 (yellow) for **PTZ-TPE-1, PTZ-TPE-2, PTZ-TPE-3** and **PTZ-**

TPE-4, respectively. The emission spectra of **PTZ-TPE-1** and **PTZ-TPE-3** shows large bathochromic shift and noticeable color change (Fig. 3.7 e) compared to the **PTZ-TPE-2** and **PTZ-TPE-4** as the solvent polarity increased which indicates better D-A characteristics of **PTZ-TPE-1** and **PTZ-TPE-3**.

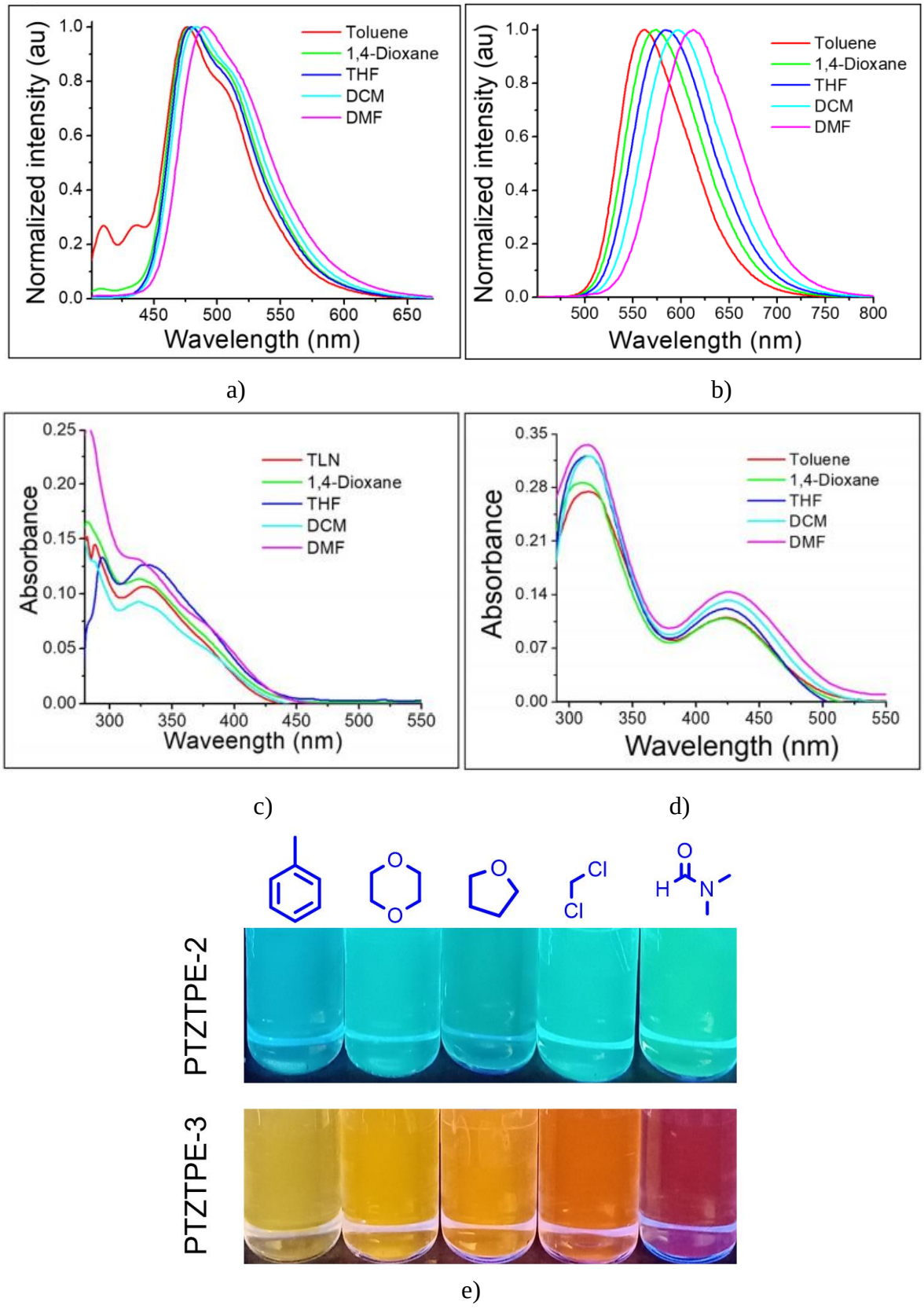

Fig. 3.7 Emission spectra of (a) **PTZ-TPE-2**, (b) **PTZ-TPE-3** and absorbtion spectra of (c) **PTZ-TPE-2**, (d) **PTZ-TPE-3** in different polarity solvents, (e) Photograph of **PTZ-TPE-2** and **PTZ-TPE-3** in different polarity solvents (from toluene to DMF).

3.2.3. Triplet harvesting

In order to investigate triplet states influence for the overall luminescence of the studied compounds, PL and PL decay time measurements were performed before and after deaeration of the toluene solution (see Fig 3.8). After deaeration all four toluene solutions of the studied compounds were characterized by the identical PL spectra maxima and shape as before deaeration what indicates that in all four cases origin of the photoluminescence is the same stable excited singlet state. The PL intensities of **PTZ-TPE-1, PTZ-TPE-3, PTZ-TPE-3** and **PTZ-TPE-4** deaerated solutions in toluene were 1.05, 1.03, 1.06 and 1.28 times higher respectively (Fig. 3.7 a). While PL decay times were relatively short and were not influenced by the presence of air. PL decays of **PTZ-TPE-1, PTZ-TPE-3, PTZ-TPE-3** and **PTZ-TPE-4** deaerated solutions in toluene were found to be 1.04, 1.01, 1.09 and 1.06 times longer respectively (Fig. 3.7 b). Such results show that for all studied phenothiazine substituted tetraphenylethylenes dominant luminescence mechanism is a prompt fluorescence and triplet excited states do not have noticeable influence for the overall luminescence of the compounds.

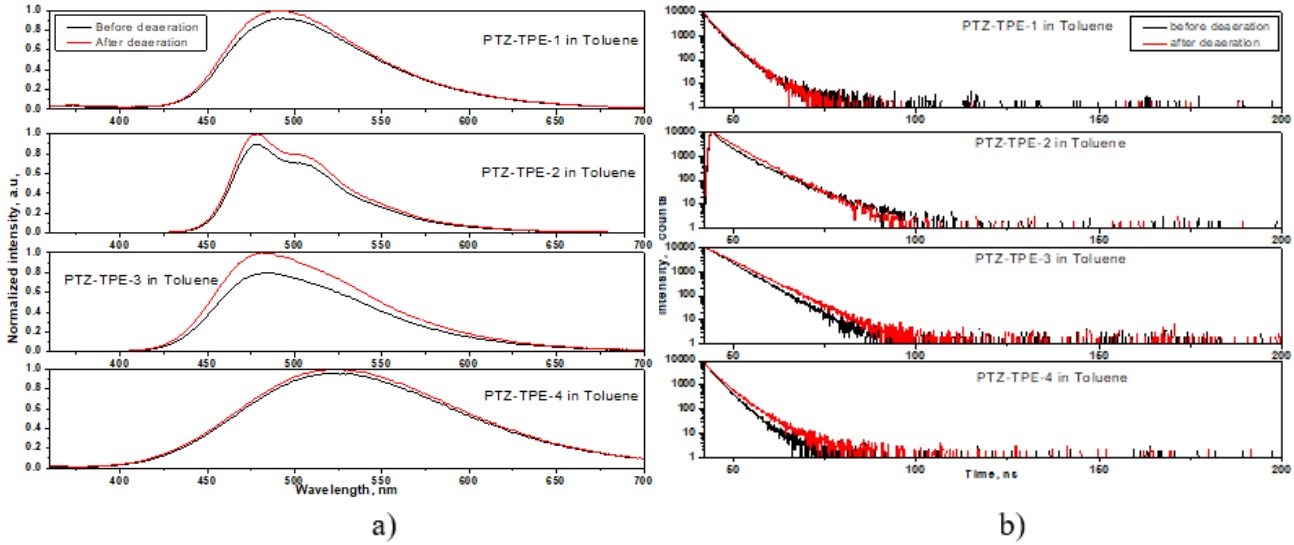

Fig. 3.8 a) PL spectra and b) PL time decays of air-free and non-deoxygenated **PTZ-TPE-1, PTZ-TPE-2, PTZ-TPE-3** and **PTZ-TPE-4** solutions in toluene

3.2.4. Aggregation enhanced emission

Because of PLQY measurements results and the fact that phenothiazine substituted tetraphenylethylenes is known for their AIE/AIEE active behavior, AIE study was performed. All studied compounds were dissolved in water and THF mixture with different amounts of water fraction ranging from 0 to 95% by volume (see Fig. 3.9 and Fig 3.10). The images of the phenothiazine substituted tetraphenylethylenes derivatives in THF–water mixtures with various water fractions under UV illumination are shown in Fig. 3.9.

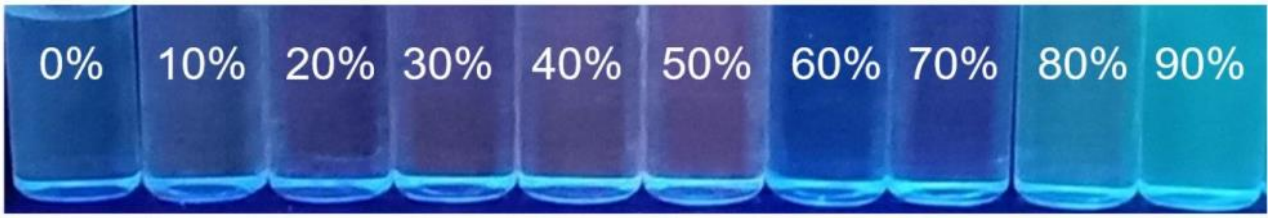

a)

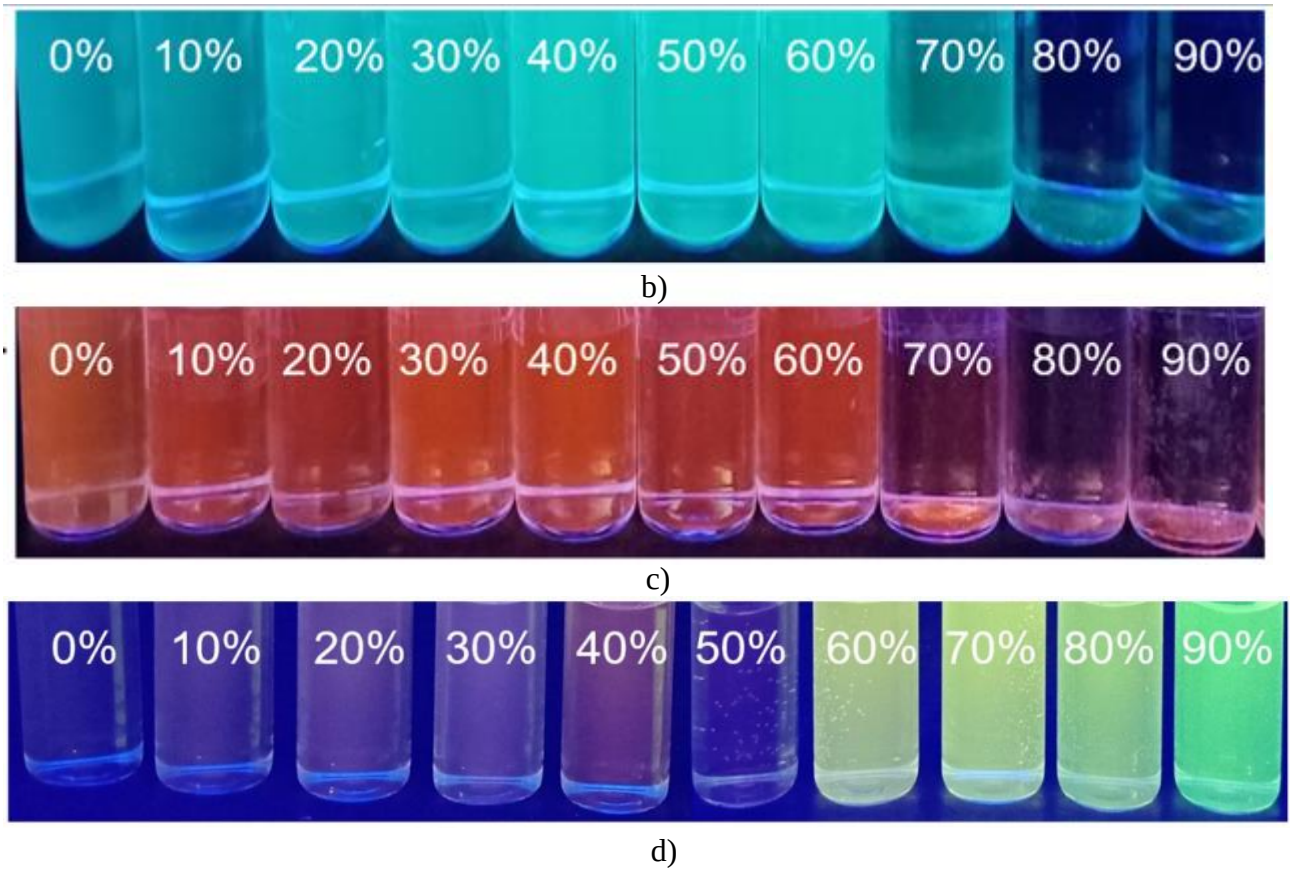

Fig. 3.9 Photographs of compounds (a) **PTZ-TPE-1**, (b) **PTZ-TPE-2**, (c) **PTZ-TPE-3** and (d) **PTZ-TPE-4** in different THF- water mixtures taken under 365 nm UV illumination.

Compounds **PTZ-TPE-1** and **PTZ-TPE-4** showed only weak emission at low water percentages (under 60% and 50%, respectively) caused by free phenyl ring rotation resulting in energy loss in non-radiative way. After water concentration reached more than 60% molecules starts to form bigger aggregates which results in free phenyl ring rotation restriction and enhancement of the emission intensity (see Fig. 3.10 a, d). On the other hand, compounds **PTZ-TPE-2** and **PTZ-TPE-3** were characterized by noticeable fluorescence at low water concentration due to cyano groups. In case of compound **PTZ-TPE-2**, while water fraction in the mixtures is lower than 60% fluorescence intensity of continuously increases with increasing water fraction (see Fig. 3.10 b). However, PL intensity starts to decrease at further increase of water fraction when its concentration exceeds 60%. Results show that while water concentration is lower than 60% limit, compound **PTZ-TPE-2** also forms nano-aggregates which restricts rotation of phenyl rings via single bonds. However, at high water concentrations fluorescence intensity decreases due to formation of even bigger aggregates which results that only surface molecules of those aggregates are capable to emit light and contribute to the overall fluorescence intensity leading to a decrease of the emission intensity. In case of compound **PTZ-TPE-3**, highest fluorescence intensity was measured in pure THF solution while intensity of the emission decreased with each increase of water content in the mixture (see Fig. 3.10 c). Because of that it can be concluded that compound **PTZ-TPE-3** is characterized by aggregation-caused quenching (ACQ) which is common phenomena for most organic emitters. The ACQ behavior of **PTZ-TPE-3** can be explained by π-π stacking which decreases the emission intensity of the compound in aggregated state, therefore **PTZ-TPE-3** shows a regular decrease in the emission intensity as the content of water increases. The **PTZ-TPE-1, PTZ-TPE-3, PTZ-TPE-3** and **PTZ-**

TPE-4 emit at 539 nm, 482 nm, 585 nm and 574 nm respectively in pure THF solution. However, if water fraction in the mixture is lower than 50% emission peaks demonstrate bathochromic shift under water fraction increase. This behavior is the same as in case of solvatochromism study and can be explained by stabilization of the excited states due to increase in polarity.

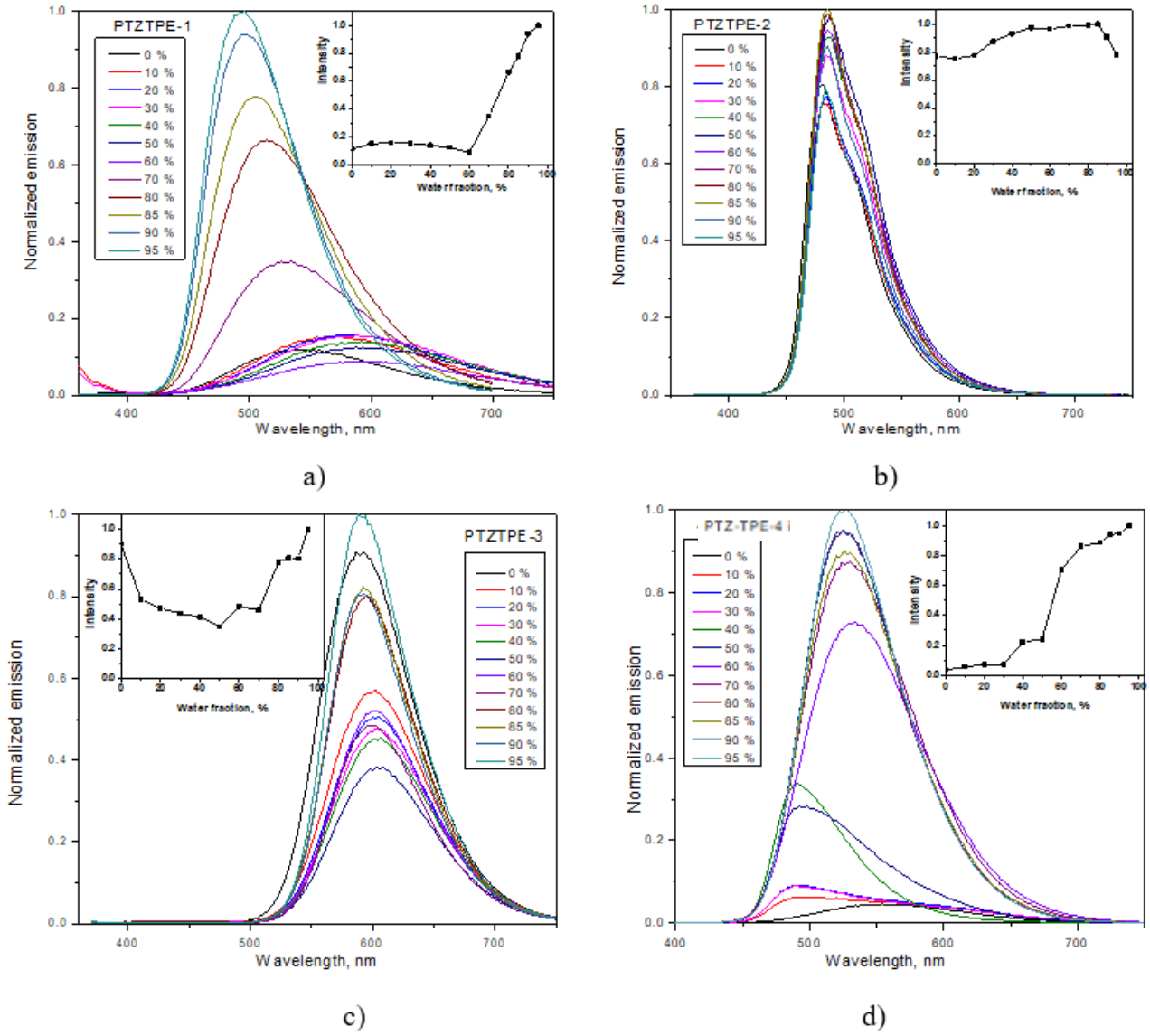

Fig. 3.10 Emission spectra of the investigated compounds in THF/H2O mixtures containing different water fractions.

3.2.5. Hyperfluorescence

In order to find working hyperfluorescence system which later could be used in OLEDs fabrication following study was done. In order to create working hyperfluorescence structure need to find three components: emitter, co-host and matrix or main host. Since studied compounds were characterized by prompt fluorescence they will be used as emitters, TADF compound pCNBCz0CF3 was selected as co-host while mCP was used as a matrix. The selection of co-host and main host was argumented according to the requirements for hyperfluorescence which was analyzed in the literature review (section 1.6). For example, $HOMO_{PTZ\text{-}TPE\text{-}3} > HOMO_{pCNBCzoCF3} > HOMO_{mCP}$ and $LUMO_{PTZ\text{-}TPE\text{-}3} < LUMO_{pCNBCzoCF3} < LUMO_{mCP}$. Firstly, to ensure effective Foster energy transfer spectral overlap between studied compounds absorption and co-host emission spectra was investigated (see Fig. 3.11

a). The best absorption-emission spectral overlap of co-hosts:emitter systems was found for compound **PTZT-PE-3**, while **PTZ-TPE-2** did not pass energy levels requirements and was not selected for the fabrication of hyperfluorescence systems. In order to find optimal emitter and co-host concentrations, PL spectra of fabricated hyperfluorescence structures were investigated. In that way optimized concentration of 2:15:83wt% for spin-coated **PTZ-TPE-1**: pCNBCz0CF3 :mCP, **PTZ-TPE-3**: pCNBCz0CF3 :mCP and **PTZ-TPE-4**: pCNBCz0CF3 :mCP films with hyperfluorescence properties were developed. Fig. 3.11 b shows developed **PTZ-TPE-1**: pCNBCz0CF3 :mCP, **PTZ-TPE-3**: pCNBCz0CF3 :mCP and **PTZ-TPE-4**: pCNBCz0CF3 :mCP films PL spectra. On case of **PTZ-TPE-3** and **PTZ-TPE-4** it is clearly visible that emission of the system is completely related to emission of compounds studied compounds showing efficient energy transfer from co-hosts to the low concentrated emitter. However, structure containing **PTZ-TPE-1** shows emission related to both pCNBCz0CF3 and itself. It can be explained by small spectral overlap which results in less efficient Foster energy transfer. Moreover, in comparison to the prompt fluorescence lifetimes, PL decays of developed hyperfluorescence structures were characterized by noticeably longer lifetimes (see Fig. 3.11 c). It can be explained by the presence of the RISC process of TADF co-host pCNBCz0CF3 which is necessary for hyperfluorescence to happen.

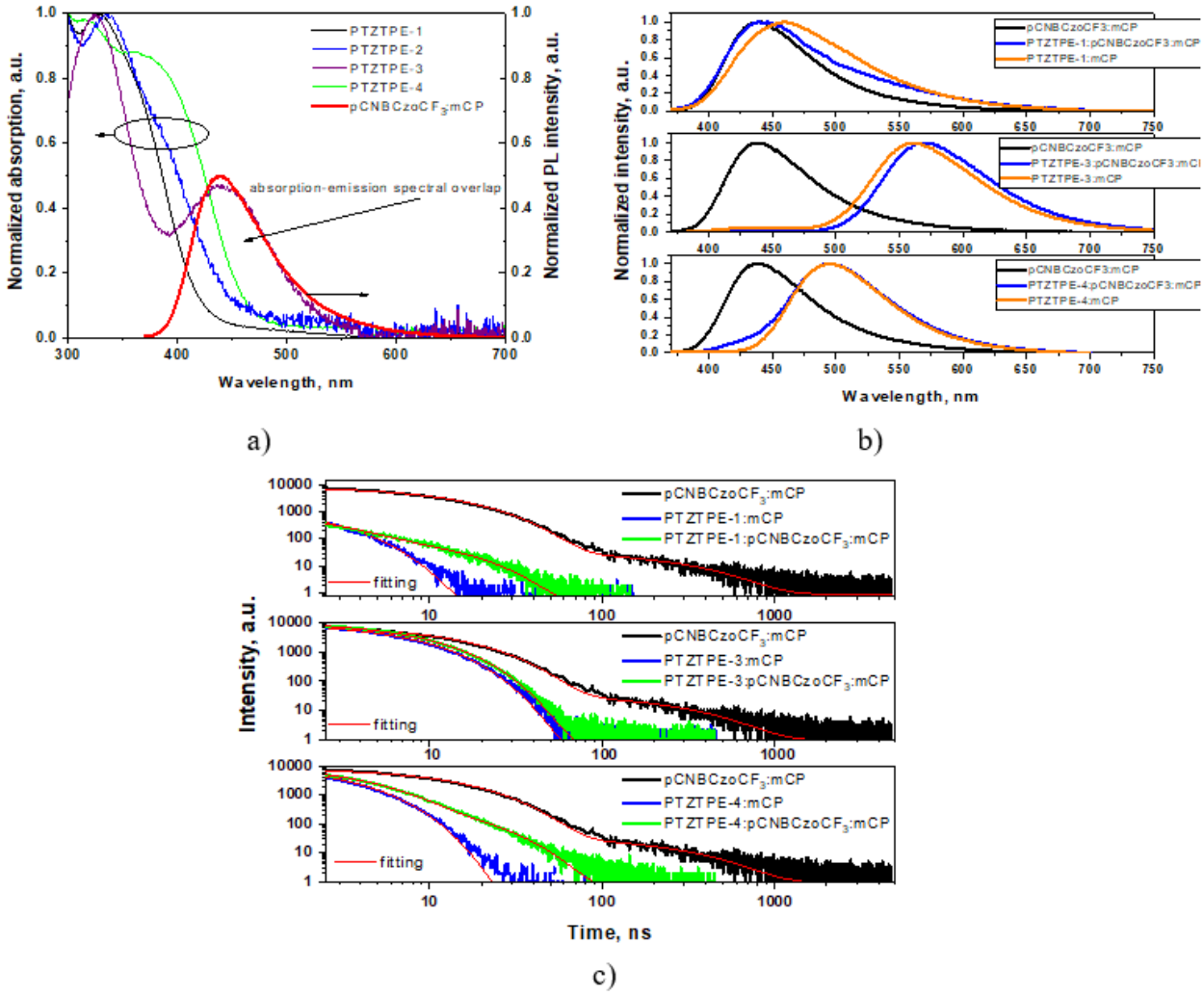

Fig. 3.11 (a) Absorption spectra of the studied compounds films and PL spectrum of co-hosts pCNBCzoCF$_3$:mCP in solid-state, (b) PL spectra, (c) PL decay lifetimes of developed hyperfluorescence structures

Measured PL decays were fitted exponentially. All fitting results are presented in Table 4. TADF emitter pCNBCz0CF3 was characterized by two time components of 12.44ns and 253.21ns. In case of all developed structures, lifetime of main luminescence contributor is much lower and are in a good agreement with prompt fluorescence lifetimes of the studied compounds. As mentioned before compound **PTZ-TPE-3** was characterized by biggest spectral overlap which causes the most efficient FRET resulting that the system **PTZ-TPE-3**: pCNBCz0CF3 :mCP was fitted by one time component of 6.7 ns. Other systems – **PTZ-TPE-1**: pCNBCz0CF3 :mCP and **PTZ-TPE-4**: pCNBCz0CF3 :mCP systems were fitted by two time components (Fig. 3.11 c, Table 4). Fitting results were in good agreement with PL spectra measurements. Structure **PTZ-TPE-1**: pCNBCz0CF3 :mCP was characterized by two equally relevant time components (55.47% and 44.53%), while structure **PTZ-TPE-4**: pCNBCz0CF3 :mCP was characterized by one dominant component of prompt fluorescence (80.25%) and second time component coming from pCNBCz0CF3 which is longer and has 5 times smaller influence for overall luminescence. PL decay fitting and PL spectra results allow to conclude that all developed structures are working by hyperfluorescence mechanism where main contributor of the overall luminescence is prompt fluorescence coming from studied compounds.

Table 4. PL decay fitting results for the studied hyperfluorescence structures.

	t_1, ns	Influence %	t_2, ns	Influence %	χ^2
pCNBCzoCF$_3$:mCP (15:85 wt%)	12.44	92.21	253.21	7.79	1.12
PTZTPE-1:mCP (10:90wt%)	1.79	100	-	-	0.94
PTZTPE-1: pCNBCzoCF$_3$:mCP (2:15:83wt%)	1.8	55.47	9.54	44.53	1.04
PTZTPE-3:mCP (10:90wt%)	5.89	100	-	-	1.07
PTZTPE-3: pCNBCzoCF$_3$:mCP (2:15:83wt%)	6.7	100	-	-	0.93
PTZTPE-4:mCP (10:90wt%)	2.41	100	-	-	1.08
PTZTPE-4: pCNBCzoCF$_3$:mCP (2:15:83wt%)	2.95	80.25	12.23	19.75	1.14

* χ^2 - fitting accuracy parameter

3.3. Electroluminescent properties

Experiment results showed that studied compounds can be used in OLEDs due to their photophysical, electrochemical, and electrooptical properties. Several types of devices were developed, fabricated, and characterized in order to study the electroluminescent properties of **PTZ-TPE-1**, **PTZ-TPE-2**, **PTZ-TPE-3**, and **PTZ-TPE-4** as emitters. All constructed OLEDs can be classified into three distinct categories based on their structure and fabrication technique. Table 5 demonstrates to which type each OLED belongs. what EML each of them has and by which technique it was fabricated.

Table 5. Types of fabricated OLEDs

Device	Type	Emitting layer	Fabrication technique
PV1	I	*PTZ-TPE-1*	Vacuum deposition
PV2		*PTZ-TPE-2*	Vacuum deposition
PV3		*PTZ-TPE-3*	Vacuum deposition
PV4		*PTZ-TPE-4*	Vacuum deposition
PS1	II	*PTZ-TPE-1*	Vacuum deposition/spin-coating
PS2		*PTZ-TPE-2*	Vacuum deposition/spin-coating
PS3		*PTZ-TPE-3*	Vacuum deposition/spin-coating
PS4		*PTZ-TPE-4*	Vacuum deposition/spin-coating
HF1	III	*PTZ-TPE-1:pCNBCzoCF₃:mCP*	Vacuum deposition/spin-coating
HF3		*PTZ-TPE-3:pCNBCzoCF₃:mCP*	Vacuum deposition/spin-coating
HF4		*PTZ-TPE-4:pCNBCzoCF₃:mCP*	Vacuum deposition/spin-coating

At first, two different structures with pure EML were designed. PV series devices had structure of ITO/HAT-CN (8nm)/TCTA (32nm)/**PTZ-TPE** (24 nm)/TSPO1 (8nm)/TPBi (40nm)/LiF:Al which can be seen in Fig. 3.12 a. HAT-CN (Fig. 2.2) was utilized as a HIL, as HBL TSPO1 was employed, while TCTA and TPBi (Fig. 2.2) were used as HTL and ETL, respectively. Layers of ITO and LiF:Al played roles of anode and cathode, respectively. Another series of devices was called PS and had a structure of ITO/HAT-CN (8nm)/**PTZ-TPE** (40 nm)/TSPO1 (8nm)/TPBi (448nm)/LiF:Al which can be seen in Fig. 3.12 b. The main difference between these series is the EML fabrication technique which was used. EMLs of PV series were fabricated by vacuum deposition, while EMLs of PS series were made by spin-coating. Moreover, the HTL made of TCTA was not used in solution-processable OLEDs in order to prevent the possibility to wash it out during spin-coating of **PTZ-TPE**-based EMLs.

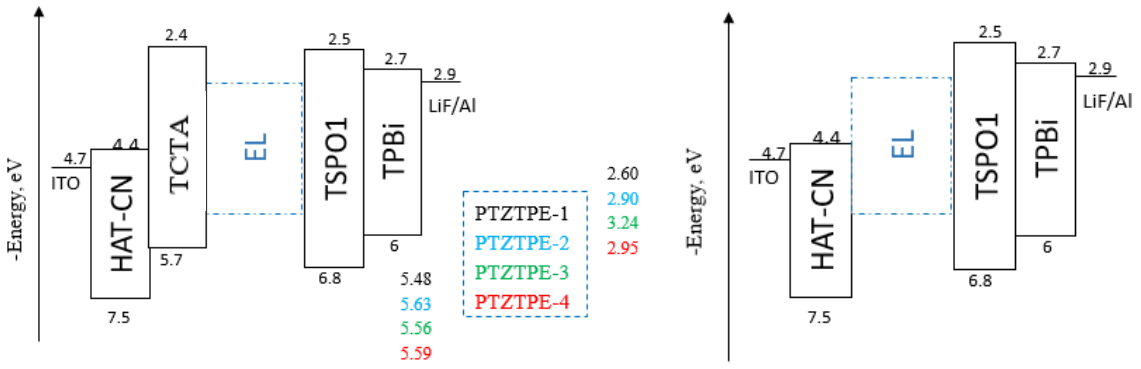

a) b)

Fig. 3.13 Energy diagram of the (a) PV and (b) PS series devices

Table 6 lists the key performance specifications of all fabricated OLEDs. The EML, which was used, is the main difference between devices of the same series (see Table 5). Based on energy levels of functional layers good charge carriers injection into EML and localization within this layers was expected. Electroluminescence spectra of PV and PS series non-doped devices showed good agreement with this expectation. Electroluminescence spectra were in the ranges of emission of **PTZ-TPEs** pure films. Moreover, under different voltages electroluminescence spectra remained stable which shows that recombination zone did not shift to the HTL or ETL. Both these observations proves good balance of fabricated devices energy levels.

Table 6. Output parameters of the **PTZ-TPEs**-based devices.

EML	Current efficiency [cd/A]	Brightness (cd/m²)	External quantum efficiency, (%)	CIE* (x, y)	CRI*
Vacuum-deposited non-doped OLEDs: ITO/HAT-CN/TCTA/**EML**/TSPO1/TPBi(40 nm)/LiF:Al					
PTZTPE-1	3.93	8055	1.07	(0.17, 0.44)	-
PTZTPE-2	2.50	3600	1.53	(0.54, 0.46)	-
PTZTPE-3	3.09	3916	1.03	(0.28, 0.47)	-
PTZTPE-4	5.40	4070	1.73	(0.32, 0.55)	-
Solution-processed non-doped OLEDs: ITO/HAT-CN/**EML**/TSPO1/TPBi(40 nm)/LiF:Al					
PTZTPE-1	0.70	2150	0.68	(0.16, 0.48)	-
PTZTPE-2	0.64	2720	0.29	(0.57, 0.44)	-
PTZTPE-3	1.85	2235	0.28	(0.27, 0.49)	-
PTZTPE-4	0.076	430	0.027	(0.35, 0.57)	-
Solution-processed doped OLEDs: ITO/MoO_3/TFB/**EML**/TSPO1/TPBi/LiF:Al					
PTZTPE-1: pCNBCzoCF$_3$:mCP (2:15:83wt%)	10.57	940	3.9	(016, 0.10)	-
PTZTPE-3: pCNBCzoCF$_3$:mCP (2:15:83wt%)	21.68	3400	8.2	(0.28, 0.38)	67
PTZTPE-4: pCNBCzoCF$_3$:mCP (2:15:83wt%)	0.87	2200	0.7	(0.17, 0.21)	-

PV series OLEDs had EQE values ranging from 1.03 to 1.73 percent (see Table 6). If we are taking into account that in case of optimized device structure charge balance factor γ=1, ratio $\eta_{S/T}$ of conventional fluorescent emitters equal to 0.25 and outcoupling efficiency $\eta_{out}\approx 0.2$, these results are in good a agreement with PLQY values of the pure layers of studied compounds (24 % for **PTZ-TPE-1**, 28 % for **PTZ-TPE-2** and **PTZ-TPE-3** and 19 % for **PTZ-TPE-4**) according to the formula 1.6. However, EQE values of PS series OLEDs were found to be noticeably lower due to the fact that the HTL was not used in these structures resulting in charge balance factor γ decrease. In comparison to device PV4, which also was based on compound **PTZ-TPE-**4, device PS4 had an extremely low EQE of 0.027 percent. It can be explained by poor solubility of the compound which leads to the bad quality of spin-coated EML**.** Overall best results in IP series showed devices PV4 and PV2 while PS1 and PS2 were best in the PS series. Worst characteristics showed device PS4 reason of which was explained before. PV1 device had the highest brightness of 8055 cd/m^2 at 18V which is 18.7 times higher than the brightness of PS2 which had the lowest brightness at the same voltage. The maximum current efficiency of 5.40 cd/A and 3.93 cd/A, power efficiency of 2.65 lm/W and 0.90 lm/W were recorded for PV4 and PV1 devices, respectively, while highest EQE of 1.73% and 1.53% were calculated for PV4 and PV2. Such different properties of **PTZ-TPE-1, PTZ-TPE-2, PTZ-TPE-3** and **PTZ-TPE-4** are related to differences in their molecular structure. Compound **PTZ-TPE-3** showed overall worst performance of OLEDs due to its structure which is not capable of AIEE, while compound **PTZ-TPE-4** demonstrated poor performance in spin-coated devices due to its big

molecule size and non-polar nature which results in poor film-forming properties. It also can be noted that position of electron-accepting cyano groups did not have noticeable influence on device performances. Figure 3.13 shows a comparison of EQE, current performance, current density, brightness, electroluminescence spectra at 9V for PS and PV series devices.

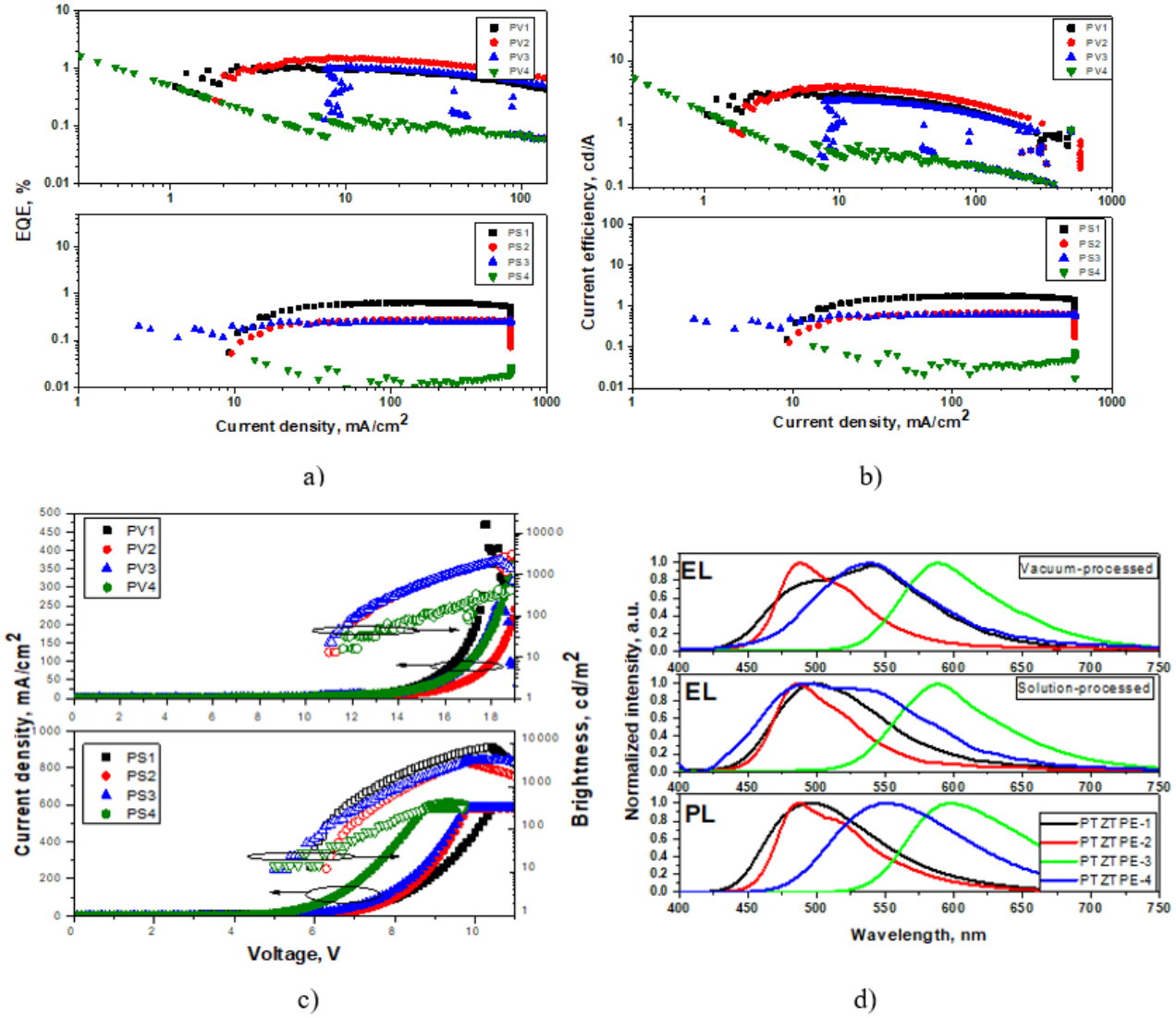

Fig. 3.14 (a) EQE dependence on current density, (b) Current efficiency dependence on current density, (c) Current density and brightness dependence on voltage, (d) Electroluminescence spectra at 9V of PV and PS series

Figure 3.14 shows a CIE 1931 color diagram of PV series devices. The CIE color coordinates of the vacuum-processed non-doped OLEDs are related to greenish-blue for **PTZ-TPE-2** (0.54; 0.46)**,** green for **PTZ-TPE-1** (0.17; 0.44)**,** yellowish-green for **PTZ-TPE-4** (0.28; 0.47), and orange for **PTZ-TPE-3** (0.32; 0.55) which all are in the range of pure films luminescence.

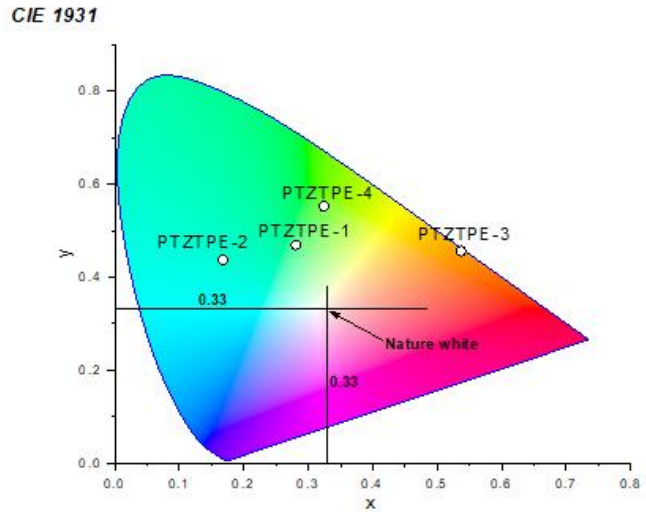

Fig. 3.15 CIE color coordinates of PV series devices

After characterization of PV and PS series was done, it was decided to optimize structure of the fabricated devices. Since AIE study showed that compounds **PTZ-TPE-1** and **PTZ-TPE-4** demonstrate stronger emission once concentration of them is high while compounds **PTZ-TPE-2** and **PTZ-TPE-3** showed only weak ACQ, usage of the host in the EML would only slightly increase the EQEs of the tetraphenylethylenes-based devices. As a result, increasing the efficiency of exciton output from χ=0.25 to χ=1 was the best way to increase overall system efficiency. In order to do that hyperfluorescence devices were fabricated. All devices had structure of ITO/MoO_3(8nm)/TFB(40nm)/EML(40nm)/TSPO1(8nm)/TPBi(40nm)/LiF:Al the energy diagram of which is schematically presented in Fig. 3.16. Doped **PTZT-PE-1**: pCNBCz0CF3 :mCP, **PTZ-TPE-3**: pCNBCz0CF3 :mCP and **PTZ-TPE-4**: pCNBCz0CF3 :mCP films with optimized concentration of 2:15:83wt% for emitter, TADF co-host and and host, respectively, were fabricated by spin-coating technique and used as EMLs in HF series devices. In case of all HF series devices new TFB layer was introduced. TFB layer played a role of HTL and EBL due to its high electron affinity (2.3 eV), high hole mobility (2×10^{-3} cm^2/Vs at the electric field of 2.5×10^5 V/cm) and low ionization potential (5.3 eV) [68]. In addition, differently than in PV and PS series in place of HAT-CN MoO_3 was used as HLT due to its non-solubility in organic solvents. The main output specifications of HF series devices are shown in Table 6.

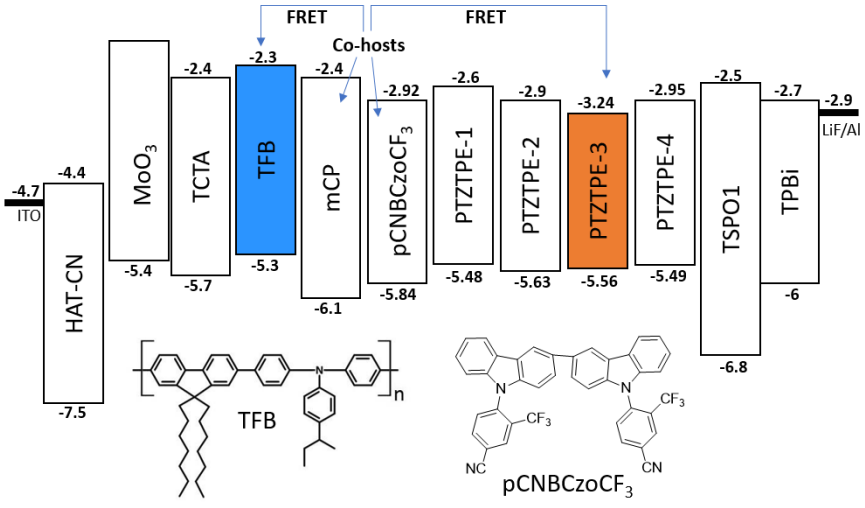

Fig. 3.16 Energy diagram of HF series devices

Basic mechanism of HF series devices is shown in Fig 3.17. Besides roles of HTL and EBL compound TFB worked as additional emitter too. It was predicted that mixing of orange hyperfluorescence of **PTZ-TPE**: pCNBCz0CF3 :mCP with blue emission TFB will result in white electroluminescence similarly to number of devices which were reported in the past [69]–[71]. However, this my suggested approach is unique in a way that emission comes from two separate layers while in case of most other white OLEDs emission comes from different emitters in the single EML. In case of this two EMLs approach we have more control under emission mechanism and optimization parameters which enables more ways to create different structures. Structure of HF series devices was designed in a way that orange emission of **PTZ-TPE-3** would overlap with blue emission of TFB with similar intensities. Injected hole-electron pairs recombine within the hyperfluorescent layer on mCP and TADF co-hosts as a result of EBL and HBL implementation, creating both singlet and triplet excitons. Due to RISC of pCNBCz0CF3 triplets then are converted into singlets. After that, singlet excitons can be transferred from host to TFB emitter or from TADF compound pCNBCz0CF3 to **PTZ-TPE** via FRET (see Fig. 3.17). Simultaneous radiative decay results in double-layered emission.

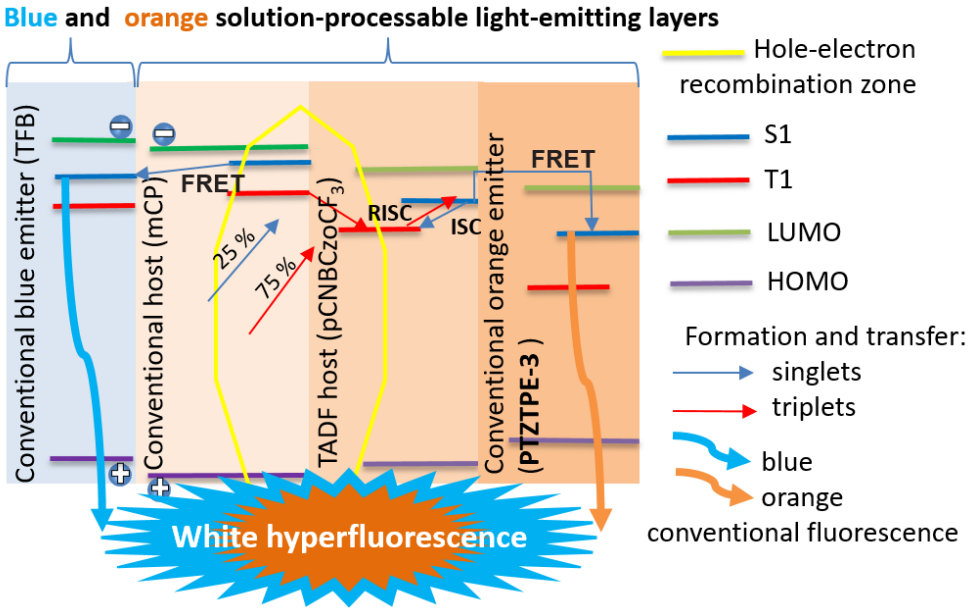

Fig. 3.17 Schematic of HF series devices working principle

Maximum EQEs of HF series solution-processable devices were much improved in comparison to EQEs of non-doped **PTZ-TPEs**-based spin-coated PS series devices due to good hole-electron balance in the EML and hyperfluorescence phenomenon resulting in high exciton output performance (Fig. 3.18 a, Table 6). Maximum current efficiency of 21.68 cd/A, power efficiency of 10.47 lm/W and EQE of 8.2% were recorded for HF3 device with compound **PTZ-TPE-3** inside the EML. This device also was characterized by lowest turn-on voltage of 4.5V. This result of device HF3 is mainly related to the high overlap of **PTZ-TPE-3** absorption and TADF co-host emission spectra (see Fig. 3.11 a) which results in the most efficient FRET. Electroluminescence spectra of device HF3 was characterized by CIE1931 color coordinates ((0.28, 0.38) at 6V) which are close to the CIE1931 color coordinates (0.33, 0.33) of nature white (see Fig. 3.18 d). White hyperelectroluminescence of HF3 was also characterized by good CRI value of 67 at 6V which was quite stable in all 5 to 9V range. Electroluminescence spectra form of HF3 remains stable under the range of voltage too. However, intensity of TFB electroluminescence part relatively slowly increasing with increase of applied voltages (see Fig. 3.18 b). It can be explained in a way that under higher voltage electrons overcome

LUMO/LUMO barrier on TFB/EML interface resulting in direct hole-electron recombination in TFB layer which lead to slight increase of TFB electroluminescence band. Since other studied compounds were characterized by higher charge mobility than **PTZ-TPE-3**, they demonstrate even higher color stability. However, their electroluminescence spectra are not completely white since their emission spectra is too close to emission spectra of TFB layer. Device HF4 with compound **PTZ-TPE-4** was characterized by lowest EQE of 0.7% while current efficiency was more than 25 times lower in comparison to HF3. Similarly to PS series, efficiency of **PTZ-TPE-4**: pCNBCz0CF3 :mCP-based device was much lower than efficiencies other HF series devises. It can be explained by poor **PTZ-TPE-4** solubility resulting in poor film forming properties then it is formed by spin-coating technique. Figure 3.18 shows a complete comparison of EQE, CIE coordinates, brightness, current density, and electroluminescence spectra for HF series devices at various voltages.

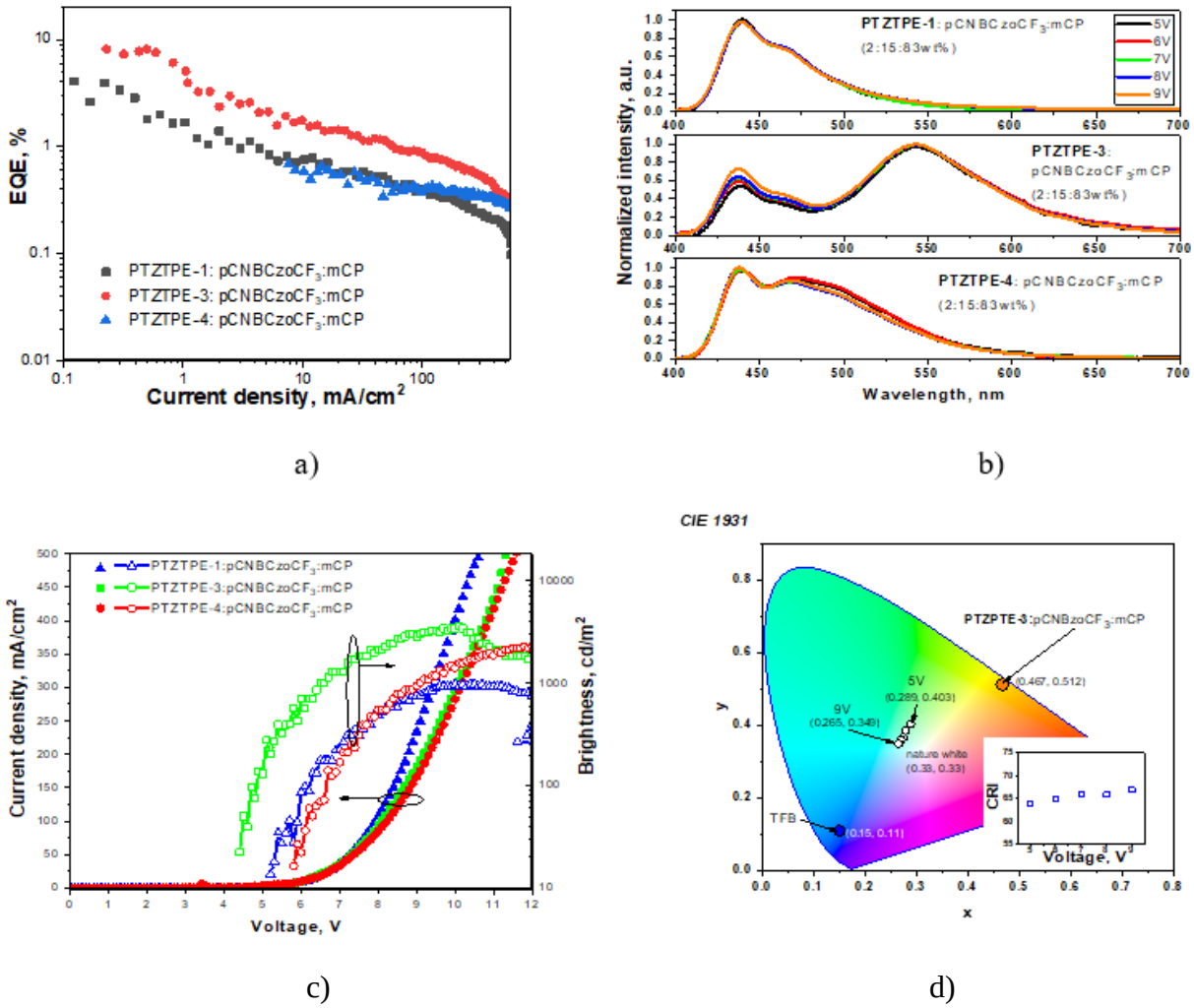

Fig. 3.18 (a) EQE dependence on current density (b) Electroluminescence spectra at 9V of HF series devices, (c) Current density and brightness dependence on voltage, (d) CIE1931 colour coordinates of TFB layer, **PTZ-TPE-3**:pCNBCzoCF$_3$:mCP layer, HF3 electoluminiscence under different voltages and CRI of HF3 dependence on voltage

Conclusions

1. Influence of number of phenothiazine substitutes and cyano group position of compounds **PTZ-TPE** was investigated on their photophysical properties. Studied compounds **PTZ-TPE-1 and PTZ-TPE-4** without cyano groups demonstrated **aggregation enhanced prompt fluorescence** while compounds with cyano group were not characterized by **aggregation induced emission enhancement**.

2. Studied **PTZ-TPE** compounds were characterized by higher than 60 % PLQY values and colors falling in 482-585nm range in their low-polarity toluene solution, while under increase of solvent polarity **PTZ-TPE-3** showed biggest red shift in its emission compared to the other studied compounds which indicates donor-acceptor character of this compound ;

3. Charge injecting/transporting properties of solid films of compounds were investigated by electron photoemission spectrometry and time of flight measurements showing that the studied compounds can be used in organic light emitting diodes fabrication Ionization potentials were found to be between 5.48-5.63 eV while maximum hole mobility reached 1.67×10^{4} $cm^{2}V^{-1}s^{-1}$ at 4.6×10^{5} V/cm electric field;

4. According to the provided **PTZ-TPE** compounds characterizations, they were used in organic light emitting diodes as emitters. Non-doped devices based on novel emitters **PTZ-TPE** demonstrated external quantum efficiency up to 1.73%. While, hyperfluorescence devices based on **PTZ-TPE** as emitters and pCNBCz0CF3 as co-host were characterized by external quantum efficiency up to 8.2 % and close to natural white CIE coordinates of (0.28, 0.38).

5. Suggested novel **hyperfluorescence** emission structures tremendously improved performance of organic light emitting diodes in comparison to devices with pure solution-processed emitting layers, external quantum efficiency improvement reaching from 0.28% to 8.2%.

6. The best hyperfluorescence device performances were obtained for devices based on **PTZ-TPE-3** which were characterized by biggest 141 nm spectral overlap with co-host, low-dispersity charge-transport properties and appropriate levels of lowest unoccupied molecular orbital (3.24 eV) and highest occupied molecular orbital (5.5 eV).

List of references

[1] C. W. Tang and S. A. Vanslyke, “Organic electroluminescent diodes,” *Appl. Phys. Lett.*, 1987, doi: 10.1063/1.98799.

[2] S. Juršėnas, *Organinės optoelektronikos prietaisai*. Vilnius: Progretus, 2008.

[3] G. A. Turnbull, Y. Yang, A. E. Vasdekis, A. Ruseckas, and I. D. Samuel, “Organic Semiconductor Lasers,” *ECS Trans.*, vol. 25, no. 7, 2019, doi: 10.1149/1.3203990.

[4] I. Gallardo, G. Guirado, J. Hernando, S. Morais, and G. Prats, “A multi-stimuli responsive switch as a fluorescent molecular analogue of transistors,” *Chem. Sci.*, vol. 7, no. 3, 2016, doi: 10.1039/c5sc03395k.

[5] A. Kishimura, T. Yamashita, K. Yamaguchi, and T. Aida, “Rewritable phosphorescent paper by the control of competing kinetic and thermodynamic self-assembling events,” *Nat. Mater.*, vol. 4, no. 7, 2005, doi: 10.1038/nmat1401.

[6] Z. Chi *et al.*, “Recent advances in organic mechanofluorochromic materials,” *Chem. Soc. Rev.*, vol. 41, no. 10, 2012, doi: 10.1039/c2cs35016e.

[7] S. Hirata and T. Watanabe, “Reversible Thermoresponsive Recording of Fluorescent Images (TRF),” *Adv. Mater.*, vol. 18, no. 20, 2006, doi: 10.1002/adma.200600209.

[8] G. M. Farinola and R. Ragni, “Electroluminescent materials for white organic light emitting diodes,” *Chem. Soc. Rev.*, vol. 40, no. 7, 2011, doi: 10.1039/c0cs00204f.

[9] S. Ahmad, “Organic semiconductors for device applications: Current trends and future prospects,” *J. Polym. Eng.*, vol. 34, no. 4, pp. 279–338, 2014, doi: 10.1515/polyeng-2013-0267.

[10] M. Intelligence, “OLED PANEL MARKET - GROWTH, TRENDS, COVID-19 IMPACT, AND FORECASTS (2021 - 2026),” 2021. https://www.mordorintelligence.com/industry-reports/oled-panel-market (accessed Mar. 20, 2021).

[11] B. Valeur, *Molecular Fluorescence. Principles and Applications*, vol. 8. Wiley-VCH, 2001.

[12] T. Tsutsui, “Progress in electroluminescent devices using molecular thin films,” *MRS Bull.*, vol. 22, no. 6, 1997, doi: 10.1557/S0883769400033613.

[13] X. Chen *et al.*, “Versatile Room-Temperature-Phosphorescent Materials Prepared from N-Substituted Naphthalimides: Emission Enhancement and Chemical Conjugation,” *Angew. Chemie - Int. Ed.*, 2016, doi: 10.1002/anie.201601252.

[14] C. Mayr, T. D. Schmidt, and W. Brütting, “High-efficiency fluorescent organic light-emitting diodes enabled by triplet-triplet annihilation and horizontal emitter orientation,” *Appl. Phys. Lett.*, vol. 105, no. 18, pp. 57–60, 2014, doi: 10.1063/1.4901341.

[15] F. B. Dias *et al.*, “Triplet harvesting with 100% efficiency by way of thermally activated delayed fluorescence in charge transfer OLED emitters,” *Adv. Mater.*, vol. 25, no. 27, pp. 3707–3714, 2013, doi: 10.1002/adma.201300753.

[16] H. Nakanotani *et al.*, “High-efficiency organic light-emitting diodes with fluorescent emitters,” *Nat. Commun.*, 2014, doi: 10.1038/ncomms5016.

[17] T. Furukawa, H. Nakanotani, M. Inoue, and C. Adachi, “Dual enhancement of electroluminescence efficiency and operational stability by rapid upconversion of triplet excitons in OLEDs,” *Sci. Rep.*, 2015, doi: 10.1038/srep08429.

[18] H. Mustroph, “Potential-Energy Surfaces, the Born–Oppenheimer Approximations, and the Franck–Condon Principle: Back to the Roots,” *ChemPhysChem*, 2016, doi: 10.1002/cphc.201600243.

[19] Y. Chen, L. Zhang, H. Wang, and W. Weinan, “Ground State Energy Functional with Hartree-Fock Efficiency and Chemical Accuracy,” *J. Phys. Chem. A*, vol. 124, no. 35, 2020, doi: 10.1021/acs.jpca.0c03886.

[20] I. Mayer and A. Hamza, “Energy decomposition in the topological theory of atoms in molecules and in the linear combination of atomic orbitals formalism: A note,” *Theor. Chem. Acc.*, vol. 105, no. 4–5, 2001, doi: 10.1007/s002140000230.

[21] C. C. J. Roothaan, “New Developments in Molecular Orbital Theory,” *Rev. Mod. Phys.*, vol.

23, no. 2, pp. 69–89, 2002, doi: 10.1103/revmodphys.23.69.
[22] A. Operamolla and G. M. Farinola, “Molecular and supramolecular architectures of organic semiconductors for field-effect transistor devices and sensors: A synthetic chemical perspective,” *European J. Org. Chem.*, vol. 2011, no. 3, pp. 423–450, 2011, doi: 10.1002/ejoc.201001103.
[23] S. Köber, M. Salvador, and K. Meerholz, “Organic photorefractive materials and applications,” *Adv. Mater.*, vol. 23, no. 41, pp. 4725–4763, 2011, doi: 10.1002/adma.201100436.
[24] A. Kavokin, J. J. Baumberg, G. Malpuech, and F. P. Laussy, *Microcavities*. Oxford University Press, 2008.
[25] J. P. Murphy, “NOVEL HYBRID PEROVSKITE COMPOSITES AND MICROSTRUCTURES : SYNTHESIS AND CHARACTERIZATION,” Montana Tech, 2018.
[26] Z. An *et al.*, “Stabilizing triplet excited states for ultralong organic phosphorescence,” *Nat. Mater.*, vol. 14, no. 7, pp. 685–690, 2015, doi: 10.1038/nmat4259.
[27] L. Wu *et al.*, “Förster resonance energy transfer (FRET)-based small-molecule sensors and imaging agents,” *Chemical Society Reviews*, vol. 49, no. 15. 2020, doi: 10.1039/c9cs00318e.
[28] S. S. Skourtis, C. Liu, P. Antoniou, A. M. Virshup, and D. N. Beratan, “Dexter Energy transfer pathways,” *Proc. Natl. Acad. Sci. U. S. A.*, vol. 113, no. 29, 2016, doi: 10.1073/pnas.1517189113.
[29] B. Valeur and M. N. Berberan-Santos, “A Brief History of Fluorescence and Phosphorescence before the Emergence of Quantum Theory,” *J. Chem. Educ.*, no. 88, pp. 731–738, 2011.
[30] S. E. Braslavsky, “Glossary of terms used in photochemistry, 3rd edition (IUPAC Recommendations 2006),” *Pure Appl. Chem.*, vol. 79, no. 3, pp. 293–465, 2007, doi: 10.1351/pac200779030293.
[31] K. V. R. Murthy and H. S. Virk, “Luminescence Phenomena: An Introduction,” *Defect Diffus. Forum*, vol. 347, no. December, pp. 1–34, 2013, doi: 10.4028/www.scientific.net/ddf.347.1.
[32] S. Schols, *Device Architecture and Materials for Organic Light-Emitting Devices*. Springer, 2011.
[33] A. Pigliucci and E. Vauthey, “Vibrational Relaxation Dynamics of Polyatomic Molecules in Solution,” *Chim. Int. J. Chem.*, vol. 57, pp. 200–203, 2006, doi: 10.2533/000942903777679406.
[34] S. Reineke and M. A. Baldo, “Room temperature triplet state spectroscopy of organic semiconductors,” *Sci. Rep.*, vol. 4, no. 1, p. 3797, May 2015, doi: 10.1038/srep03797.
[35] S. Knuts, H. Ågren, and B. F. Minaev, “Phosphorescence of aromatic molecules,” *J. Mol. Struct.*, vol. 311, pp. 185–197, 1994, doi: 10.1016/S0022-2860(10)80028-6.
[36] C. M. Marian, “Spin-orbit coupling and intersystem crossing in molecules,” *Wiley Interdiscip. Rev. Comput. Mol. Sci.*, vol. 2, no. 2, pp. 187–203, 2012, doi: 10.1002/wcms.83.
[37] W. M. Y. and Z. Eli, “Purely Organic Thermally Activated Delayed Fluorescence Materials for Organic Light-Emitting Diodes,” *Adv. Mater.*, vol. 29, no. 22, p. 1605444, 2017, doi: doi:10.1002/adma.201605444.
[38] M. Mamada, K. Inada, T. Komino, W. J. Potscavage, H. Nakanotani, and C. Adachi, “Highly Efficient Thermally Activated Delayed Fluorescence from an Excited-State Intramolecular Proton Transfer System,” *ACS Cent. Sci.*, vol. 3, no. 7, 2017, doi: 10.1021/acscentsci.7b00183.
[39] F. B. Dias, T. J. Penfold, M. N. Berberan-Santos, and A. P. Monkman, “Photophysics of Thermally Activated Delayed Fluorescence in Organic Molecules,” *Methods Appl. Fluoresc.*, p. 26, 2017, doi: 10.1142/9789813230194_0006.
[40] C. Baleizão and M. N. Berberan-Santos, “Thermally activated delayed fluorescence in fullerenes,” in *Annals of the New York Academy of Sciences*, 2008, pp. 224–234, doi: 10.1196/annals.1430.044.
[41] C. Y. Chan, L. S. Cui, J. U. Kim, H. Nakanotani, and C. Adachi, “Rational Molecular Design for Deep-Blue Thermally Activated Delayed Fluorescence Emitters,” *Adv. Funct. Mater.*, 2018, doi: 10.1002/adfm.201706023.

[42] F. Khan, E. Urbonas, D. Volyniuk, J. V. Grazulevicius, S. M. Mobin, and R. Misra, "White hyperelectrofluorescence from solution-processable OLEDs based on phenothiazine substituted tetraphenylethylene derivatives," *J. Mater. Chem. C*, vol. 8, no. 38, 2020, doi: 10.1039/d0tc03136d.
[43] D. Zhang, D. Zhang, and L. Duan, "Exploiting p-type delayed fluorescence in hybrid white OLEDs: Breaking the trade-off between high device efficiency and long lifetime," *ACS Appl. Mater. Interfaces*, 2016, doi: 10.1021/acsami.6b07107.
[44] Z. Wu *et al.*, "Management of Singlet and Triplet Excitons: A Universal Approach to High-Efficiency All Fluorescent WOLEDs with Reduced Efficiency Roll-Off Using a Conventional Fluorescent Emitter," *Adv. Opt. Mater.*, 2016, doi: 10.1002/adom.201600117.
[45] W. Song and K. S. Yook, "Hyperfluorescence-based full fluorescent white organic light-emitting diodes," *J. Ind. Eng. Chem.*, 2018, doi: 10.1016/j.jiec.2017.12.044.
[46] J. L. Brédas, J. P. Calbert, D. A. Da Silva Filho, and J. Cornil, "Organic semiconductors: A theoretical characterization of the basic parameters governing charge transport," *Proc. Natl. Acad. Sci. U. S. A.*, vol. 99, no. 9, 2002, doi: 10.1073/pnas.092143399.
[47] D. Ammermann, A. Böhler, S. Dirr, H. H. Johannes, and W. Kowalsky, "Multilayer organic light emitting diodes for flat panel displays," *AEU-Archiv fur Elektron. und Ubertragungstechnik*, vol. 50, no. 5, 1996.
[48] R. Pode and J. H. Kwon, "High Efficiency Red Phosphorescent Organic Light-Emitting Diodes with Simple Structure," in *Organic Light Emitting Diode - Material, Process and Devices*, 2011, p. 322.
[49] L. Ke, P. Chen, R. S. Kumar, A. P. Burden, and S. J. Chua, "Indium-tin-oxide-free organic light-emitting device," *IEEE Trans. Electron Devices*, vol. 53, no. 6, 2006, doi: 10.1109/TED.2006.874724.
[50] R. H. Friend *et al.*, "Electroluminescence in conjugated polymers," *Nature*, vol. 397, no. 6715. 1999, doi: 10.1038/16393.
[51] D. H. Huh, G. W. Kim, G. H. Kim, C. Kulshreshtha, and J. H. Kwon, "High hole mobility hole transport material for organic light-emitting devices," *Synth. Met.*, vol. 180, 2013, doi: 10.1016/j.synthmet.2013.07.021.
[52] Y. Sun *et al.*, "A pyridine-containing anthracene derivative with high electron and hole mobilities for highly efficient and stable fluorescent organic light-emitting diodes," *Adv. Funct. Mater.*, vol. 21, no. 10, 2011, doi: 10.1002/adfm.201002691.
[53] D. Chen, S. J. Su, and Y. Cao, "Nitrogen heterocycle-containing materials for highly efficient phosphorescent OLEDs with low operating voltage," *Journal of Materials Chemistry C*, vol. 2, no. 45. 2014, doi: 10.1039/c4tc01941e.
[54] S. Liu, B. Li, L. Zhang, H. Song, and H. Jiang, "Enhanced efficiency and reduced roll-off in nondoped phosphorescent organic light-emitting devices with triplet multiple quantum well structures," *Appl. Phys. Lett.*, vol. 97, no. 8, 2010, doi: 10.1063/1.3483131.
[55] A. G. Mückl, S. Berleb, W. Brütting, and M. Schwoerer, "Transient electroluminescence measurements on organic heterolayer light emitting diodes," *Synth. Met.*, vol. 111, 2000, doi: 10.1016/S0379-6779(99)00367-7.
[56] H. Mu, I. Reddy, J. Hunt, P. Severs, and S. Patil, "Electron mobility characterization in OLEDs from ac small signal optical modulation," *J. Phys. D. Appl. Phys.*, vol. 43, no. 19, 2010, doi: 10.1088/0022-3727/43/19/195103.
[57] K. Sato, K. Shizu, K. Yoshimura, A. Kawada, H. Miyazaki, and C. Adachi, "Organic luminescent molecule with energetically equivalent singlet and triplet excited states for organic light-emitting diodes," *Phys. Rev. Lett.*, vol. 110, no. 24, 2013, doi: 10.1103/PhysRevLett.110.247401.
[58] X. Ren, J. Li, R. J. Holmes, P. I. Djurovich, S. R. Forrest, and M. E. Thompson, "Ultrahigh energy gap hosts in deep blue organic electrophosphorescent devices," *Chem. Mater.*, vol. 16, no. 23, 2004, doi: 10.1021/cm049402m.
[59] N. C. Erickson and R. J. Holmes, "Highly efficient, single-layer organic light-emitting devices

based on a graded-composition emissive layer," *Appl. Phys. Lett.*, vol. 97, no. 8, 2010, doi: 10.1063/1.3481426.

[60] M. H. Lu and J. C. Sturm, "Optimization of external coupling and light emission in organic light-emitting devices: Modeling and experiment," *J. Appl. Phys.*, vol. 91, no. 2, pp. 595–604, 2002, doi: 10.1063/1.1425448.

[61] J. S. Kim, P. K. H. Ho, N. C. Greenham, and R. H. Friend, "Electroluminescence emission pattern of organic light-emitting diodes: Implications for device efficiency calculations," *J. Appl. Phys.*, vol. 88, no. 2, 2000, doi: 10.1063/1.373779.

[62] L. Zhao, T. Komino, M. Inoue, J. H. Kim, J. C. Ribierre, and C. Adachi, "Horizontal molecular orientation in solution-processed organic light-emitting diodes," *Appl. Phys. Lett.*, vol. 106, no. 6, 2015, doi: 10.1063/1.4907890.

[63] Edinburgh Instruments Ltd, "Quantum Yield Measurements of Powder Samples Using the Integrating Sphere." https://www.edinst.com/quantum-yield-measurements/ (accessed Apr. 17, 2021).

[64] N. A. Montgomery *et al.*, "Dynamics of fluorescence depolarisation in star-shaped oligofluorene- truxene molecules," *Phys. Chem. Chem. Phys.*, vol. 14, pp. 9176–9184, 2012, doi: 10.1039/c2cp24141b.

[65] C. A. Amorim, M. R. Cavallari, G. Santos, F. J. Fonseca, A. M. Andrade, and S. Mergulhão, "Determination of carrier mobility in MEH-PPV thin-films by stationary and transient current techniques," *J. Non. Cryst. Solids*, vol. 358, pp. 484–491, 2012, doi: 10.1016/j.jnoncrysol.2011.11.001.

[66] D. A. Jameel, "Thin Film Deposition Processes," *Int. J. Mod. Phys. Appl.*, vol. 1, no. 4, pp. 193–199, 2015, doi: 10.1557/S0883769400063879.

[67] S. Jhulki and J. N. Moorthy, "Small molecular hole-transporting materials (HTMs) in organic light-emitting diodes (OLEDs): structural diversity and classification," *Journal of Materials Chemistry C*, vol. 6, no. 31. 2018, doi: 10.1039/c8tc01300d.

[68] M. Redecker, D. D. C. Bradley, M. Inbasekaran, W. W. Wu, and E. P. Woo, "High mobility hole transport fluorene-triarylamine copolymers," *Adv. Mater.*, vol. 11, no. 3, 1999, doi: 10.1002/(SICI)1521-4095(199903)11:3<241::AID-ADMA241>3.0.CO;2-J.

[69] J. Sun *et al.*, "Charge-Transfer Exciton Manipulation Based on Hydrogen Bond for Efficient White Thermally Activated Delayed Fluorescence," *Adv. Funct. Mater.*, 2019, doi: 10.1002/adfm.201908568.

[70] C. Xue *et al.*, "Recent advances in thermally activated delayed fluorescence for white OLEDs applications," *Journal of Materials Science: Materials in Electronics*, vol. 31, no. 6. 2020, doi: 10.1007/s10854-020-03060-z.

[71] G. Grybauskaite-Kaminskiene *et al.*, "Contribution of TADF and exciplex emission for efficient 'warm-white' OLEDs," *J. Mater. Chem. C*, vol. 6, no. 6, 2018, doi: 10.1039/c7tc05392d.